



3 1176 00160 0098

NASA TM-82644

DOE/NASA/51040-30
NASA TM-82644

NASA-TM-82644

19820013319

Cold-Air Performance of a 15.41-cm-Tip-Diameter Axial-Flow Power Turbine with Variable-Area Stator Designed for a 75-kW Automotive Gas Turbine Engine

Kerry L. McLallin, Milton G. Kofskey, and Robert Y. Wong
National Aeronautics and Space Administration
Lewis Research Center

LIBRARY COPY

February 1982

APR 6 1982

LANGLEY RESEARCH CENTER
LIBRARY, NASA
HAMPTON, VIRGINIA

Prepared for
U.S. DEPARTMENT OF ENERGY
Conservation and Renewable Energy
Office of Vehicle and Engine R&D

Cold-Air Performance of a 15.41-cm-Tip-Diameter Axial-Flow Power Turbine with Variable-Area Stator Designed for a 75-kW Automotive Gas Turbine Engine

Kerry L. McLallin, Milton G. Kofskey, and Robert Y. Wong
National Aeronautics and Space Administration
Lewis Research Center
Cleveland, Ohio 44135

February 1982

Work performed for
U.S. DEPARTMENT OF ENERGY
Conservation and Renewable Energy
Office of Vehicle and Engine R&D
Washington, D.C. 20545
Under Interagency Agreement DE-AI01-77CS51040

N82-21193 #

NOTICE

This report was prepared to document work sponsored by the United States Government. Neither the United States nor its agent, the United States Department of Energy, nor any Federal employees, nor any of their contractors, subcontractors or their employees, makes any warranty, express or implied, or assumes any legal liability or responsibility for the accuracy, completeness, or usefulness of any information, apparatus, product or process disclosed, or represents that its use would not infringe privately owned rights.

Summary

Experimentally determined performance data are presented for the power turbine stage of the Department of Energy upgraded automotive gas turbine engine. The power turbine is a single-stage, axial-flow design with pivotable vanes to vary stator area for engine control and braking. The stage performance evaluation was performed with dry air at nominal stator inlet conditions of 320 K and 0.409 atmosphere. At these conditions a Reynolds number equal to that at actual engine conditions was obtained at the equivalent design values of speed and pressure ratio. The results are presented for stator throat areas of 79.3, 100.0, 117.7, and 135.6 percent of design in terms of mass flow rate, torque, speed, power, and efficiency. Stator performance is presented in terms of mass flow rate and stator exit torque, which was measured with a stationary paddlewheel rotor. Interstage duct performance and exit diffuser performance are presented in terms of wall static pressures. The results of radial surveys of flow angle, total temperature, and total pressure are presented at the stator inlet and the rotor exit.

The total efficiency of the power turbine blading at equivalent design values of speed and pressure ratio was 0.096 less than the design value of 0.85 for 100 percent of the design stator throat area. Stage efficiency (including the exit diffuser) decreased as the stator throat area was increased above design but remained nearly constant as the throat area was decreased to 79.3 percent of design. The power turbine operating line for steady-state operation along the road-load power curve fell within 0.02 of the maximum available efficiency at any given speed for both 79.3 and 100 percent of the design stator throat area.

The measured equivalent values of mass flow rate and turbine torque were 4.35 percent greater and 7.0 percent less than design, respectively, at equivalent design values of speed and pressure ratio for ambient-temperature hardware. These measured values resulted in an equivalent work output that was 11.35 percent less than design. The stator inlet survey results indicated large radial gradients in flow angle and total pressure, which were factors in the low measured turbine efficiency. The measured interstage duct and exit diffuser static pressure recoveries were 0.559 and 0.535, respectively, which were slightly less than their respective design values of 0.570 and 0.580.

Introduction

The Department of Energy (DOE) is conducting a program to demonstrate an automobile powered by a gas turbine engine with driveability characteristics and fuel economy that can compete with those of a conventionally powered automobile. A DOE contract was awarded to the Chrysler Corp. for the mechanical design, fabrication, and road demonstration of a 75-kilowatt upgraded gas turbine engine in an automobile. The engine and its design features are described in reference 1. As part of an interagency agreement with DOE the NASA Lewis Research Center has responsibility for the aerodynamic design and evaluation of the turbomachinery components.

The turbomachinery components that were designed and evaluated include the compressor, the compressor drive turbine, the interstage duct, the power turbine, and the exit diffuser. The aerodynamic designs of these components are given in references 2 to 4. This report gives the results of the performance evaluation of the variable-area-stator power turbine with interstage duct and exit diffuser as configured in the engine. The 15.41-centimeter-tip-diameter turbine is a single-stage, axial-flow design incorporating pivotable stator vanes to provide for stator area change for engine braking and control.

This report describes the cold-air performance characteristics of the power turbine obtained over a range of stator vane-chord setting angles. The evaluation was made with nominal inlet conditions of 320 K and 0.409 atmosphere. These conditions give a Reynolds number of 1.83×10^5 , which is equal to that at actual hot-engine design-point operating conditions. The Reynolds number ranged from 1.27×10^5 to 2.28×10^5 during stage tests, depending on the values of setting angle, speed, and pressure ratio. Data were obtained over a range of speeds from 0 to 130 percent of design and ratios of total to static pressure from 1.18 to 3.50. Results are expressed in terms of power, torque, mass flow, and efficiency. Results of radial surveys of rotor exit flow angle and total pressure are given at design equivalent speed and pressure ratio. In addition, performance evaluations are presented for the interstage duct and the exit diffuser. Stator performance, obtained from stator exit fluid torque measurement, is presented in terms of the total moment of tangential momentum.

Symbols

A	flow area, m^2
c	vane or blade chord, cm
D	blade surface total diffusion parameter, $2 - (W_{\text{ex}}/W_s) - (W_p/W_{\text{in}})$
ΔH	turbine specific work, J/kg
h	passage height, cm
i	incidence angle, deg
P	power, kW
p	pressure, N/cm^2
R	gas constant, for air $R = 8314.4 \text{ J/kg K}$
ΔR	passage height, cm
R_d	diffuser kinetic energy recovery, $100(\eta_7 - \eta_5)/(\eta_5' - \eta_5)$
R_t	turbine Reynolds number, $w/r\mu$
R_x	blade row reaction, $1 - (W_{\text{in}}/W_{\text{ex}})^2$
r	radius from turbine centerline, cm
S	total surface length, cm
s	vane or blade spacing, cm
T	temperature, K
U	blade speed, m/s
V	absolute velocity, m/s
W	relative velocity, m/s
w	mass flow rate, kg/s
x	local wall surface length, cm
α	absolute flow angle, deg
β	relative flow angle, deg
γ	ratio of specific heats
δ	ratio of turbine inlet total pressure to U.S. standard sea-level pressure, P_3'/P^*
ϵ	γ correction function, $0.73959/[\gamma[2/(\gamma + 1)]^{\gamma/(\gamma - 1)}]$
η	efficiency
θ	squared ratio of turbine inlet critical velocity to U.S. standard critical velocity, $(V_{\text{cr},3}/V^*)^2$
λ	work factor, $\Delta H/U_m^2$
μ	viscosity, $\text{N}\cdot\text{s}/\text{m}^2$
ρ	density, kg/m^3
τ	torque, N-m
ψ	stream function
ω	rotation speed, rad/s
Subscripts:	
cr	conditions at a Mach number of 1
eq	equivalent condition
ex	blade row exit
in	blade row inlet
m	mean section
p	pressure surface

s	suction surface
u	tangential component
x	axial component
1	station in turbine inlet plenum
2	station at interstage duct inlet downstream of preswirl vanes
3	station at interstage duct exit/stator inlet
4	station at stator exit/rotor inlet
5	station at rotor exit/diffuser inlet
6	station at diffuser exit
7	station in exit collector
Superscripts:	
'	total state condition
—	average quantity
*	value at U.S. standard sea-level conditions

Turbine Description

The subject turbine includes the interstage duct, the power turbine vanes and blading, and the exit diffuser of the DOE/Chrysler upgraded automotive gas turbine engine. The free-shaft power turbine is an axial-flow design with pivotable stator vanes to vary stator throat area for engine control and braking. A schematic of the turbine research package, figure 1, shows the aerodynamic components and support hardware as used for this performance evaluation. The duct components were included so that turbine performance could be determined for the engine flow path configuration. The preswirl vanes shown in figure 1 provide the interstage duct inlet swirl that would be produced by the compressor drive turbine operating at design point. The stator vanes, the rotor wheel, and the interstage duct struts were actual engine hardware. The rest of the hardware forming the turbine flow path was manufactured to cold dimensions modified to produce cold-setup stator end clearances and to produce cold-setup rotor tip clearances equal to the hot design value. The stator exit annulus area was 3.6 percent less than design because thermal expansion effects resulted in differences between the "hot" and "cold" dimensions.

The overall objective of the power turbine design effort was to define a turbine that would provide high efficiency, especially at low and moderate road speeds, within the geometry constraints imposed by mechanical, control, and packaging considerations. Some constraints and their impact on turbine geometry and performance are listed in table I. Additional losses were included for these constraints in determining the design efficiency potential. The turbine design-point performance is presented in table II for operation at hot, equivalent, and test conditions. The dual values shown for equivalent and

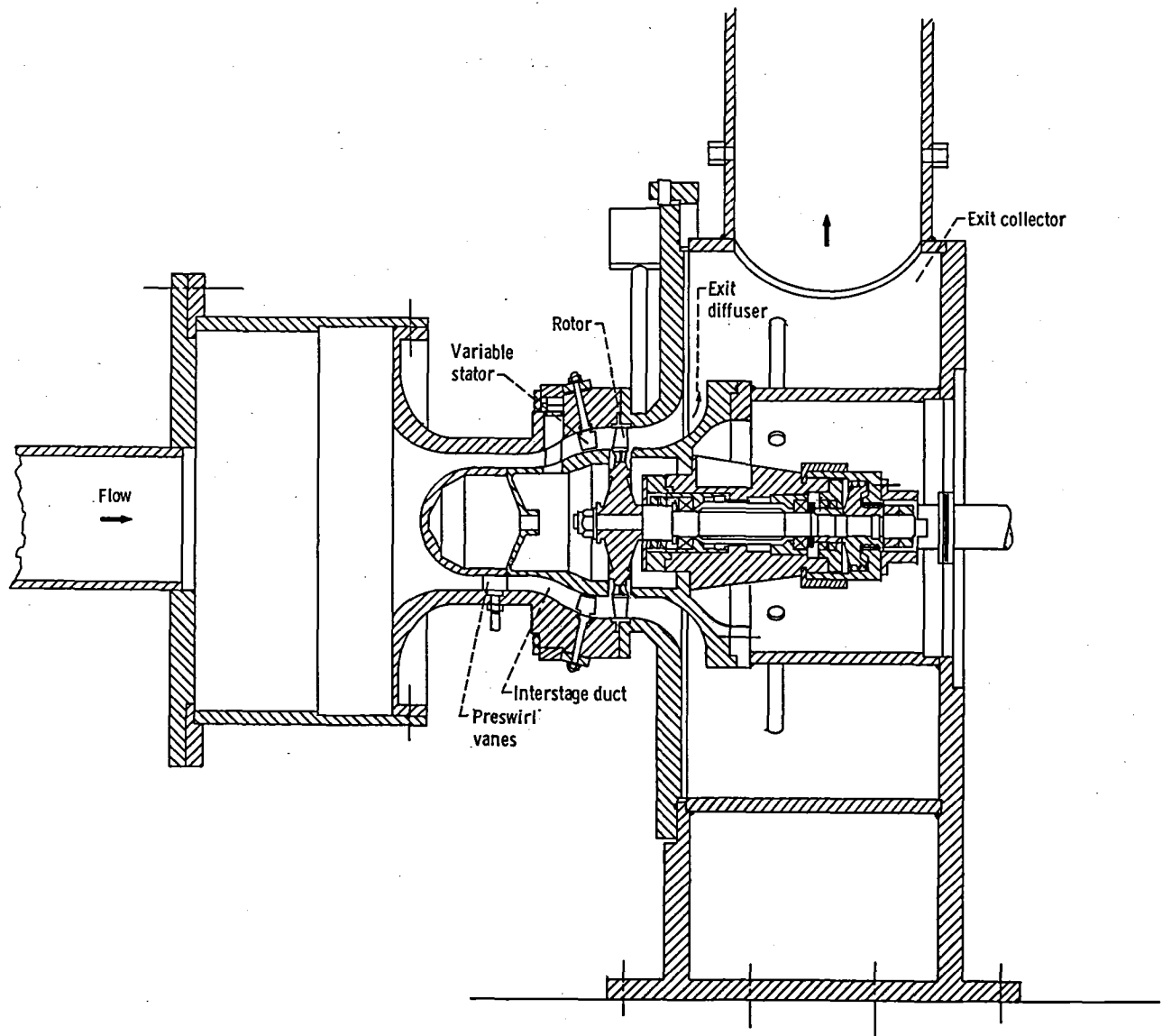


Figure 1. - Schematic of turbine used for tests.

test conditions account for changes in turbine dimensions between hot and cold operation. The design speed of 46 150 rpm is two-thirds the maximum power turbine speed. The maximum speed is where the road-load-power curve intersects the available-engine-power curve and is the speed at which the wheel stress criteria are applied to meet the 1000-hour life goal. The power turbine aerodynamic design point is not on the road-load-power curve but is the maximum unaugmented gross power (ref. 1) available at a power turbine speed of 46 150 rpm for 100 percent of gas generator speed.

The relatively high rotative speed, low overall pressure ratio, and rotor mean diameter values selected gave a low work factor of 1.247 for high efficiency potential. The losses associated with the design constraints presented in table I (low-aspect-ratio stator, stator vane-end

clearances, large rotor tip clearance, and nonuniform inlet flow conditions) resulted in a design total efficiency estimate of 0.85 for the blading. The flow coefficient V_x/U of 0.55 was selected to ensure acceptable blade root stress levels at maximum speed. The absolute flow angle at the stator exit hub was limited to 74° when the stator was in the closed position to avoid the large stator throat area variations that could occur with small errors in vane setting position. Since the variable-area stator is used for engine control, errors in vane setting position could cause large variations in the gas generator turbine inlet temperature required to maintain a given gas generator speed.

The free-stream velocity diagrams are presented in figure 2 for the hub, mean, and tip sections. These diagrams, which are based on free vortex flow, show

TABLE I. - CONSTRAINTS ON POWER TURBINE DESIGN

Constraint	Impact
Variable stator actuator mechanism packaging	Vane number limited to 23; low aspect ratio
Pivoted-vane variable-area concept	Vane-end clearances required; additional aerodynamic losses
Thermal transients during operation	Large rotor tip clearance (3 percent of blade height)
Packaging of compressor turbine and power turbine components	Long flow passage between compressor turbine rotor and power turbine stator; possible flow distortions

moderate flow turning and increasing velocities through both the stator and the rotor. The turning at the mean section is 35.2° in the stator and 80.7° in the rotor. All free-stream velocities are subsonic and the relative velocity increases across all rotor blade sections, indicating positive reaction. The mean-diameter stage reaction is 0.434 (defined as $[(W_5^2 - W_4^2)/2 \Delta H]$). The velocity diagrams were calculated by assuming a constant total pressure loss from hub to tip at both the stator exit and the rotor exit. The design relative total pressure

losses were 4.0 and 4.4 percent for the stator and the rotor, respectively.

Blading Description

The rotor and some typical stator vanes used for this performance evaluation are shown in figure 3(a). Each stator vane was integrally cast with a mounting button and a control stem. The vane stem was inserted through the shroud so that the button fit into a recess and was flush with shroud flow surface (fig. 3(b)). The vanes were actuated by a ring gear that rotated on the shroud external surface and meshed with small individual gears attached to the vane stems. The rotor was integrally cast, with the blade tips being machined to the required diameter to obtain the design hot value of tip clearance at the test conditions. The rotor was mounted on the shaft with polygon-shaped mating surfaces for torque transmission and to maintain the concentricity of the shaft and the rotor.

Stator. - The variable-area stator was designed to provide engine control and braking by using the pivotable vane concept. Since this required rotation of each vane on its pivot axis through large angles, the stator had concentric spherical end walls. The pivot axis passed through the center of the concentric spheres to allow vane rotation with constant vane-end clearance. Because of actuation mechanism constraints the number vanes was limited to 23. A larger number would be desirable from

TABLE II. - DESIGN POINT FOR THREE OPERATING CONDITIONS

Parameter	Hot condition	Equivalent condition	Test condition
Inlet total temperature, T_3' , K	1154	288.2	319.4
Inlet total pressure, P_3' , N/cm ²	19.55	10.13	4.137
Mass flow rate, kg/s	0.590	^b 0.624 ^c 0.6015	^b 0.242 ^c 0.233
Specific work, J/g	137.1	35.1	38.9
Turbine rotative speed, rpm	46 150	^b 23 343 ^c 23 576	^b 24 577 ^c 24 764
Torque, N-m	16.74	^b 8.96 ^c 8.57	^b 3.66 ^c 3.50
Rotor blade speed, U_m , m/s	331.4	167.6	176.5
Work factor, λ	1.247	1.247	1.247
Total pressure ratio, P_3'/P_5'	1.678	1.712	1.712
Static pressure ratio, P_3'/P_5	1.827	1.867	1.867
Overall static pressure ratio, P_3'/P_6	1.738	1.776	1.776
Total efficiency, η_{3-5}'	0.850	0.850	0.850
Static efficiency, η_{3-5}	0.741	0.741	0.741
Overall static efficiency, η_{3-6}	0.800	0.800	0.80
Gross power (road load, 104 km/hr), ^a kW	30.1	11.3	4.9
Gross power (design), ^a kW	80.9	^b 21.9 ^c 21.1	^b 9.41 ^c 9.08
Turbine Reynolds number, R_t	1.90×10^5	5.05×10^5	1.83×10^5

^aDesign speed.

^bHot dimensions.

^cCold dimensions.

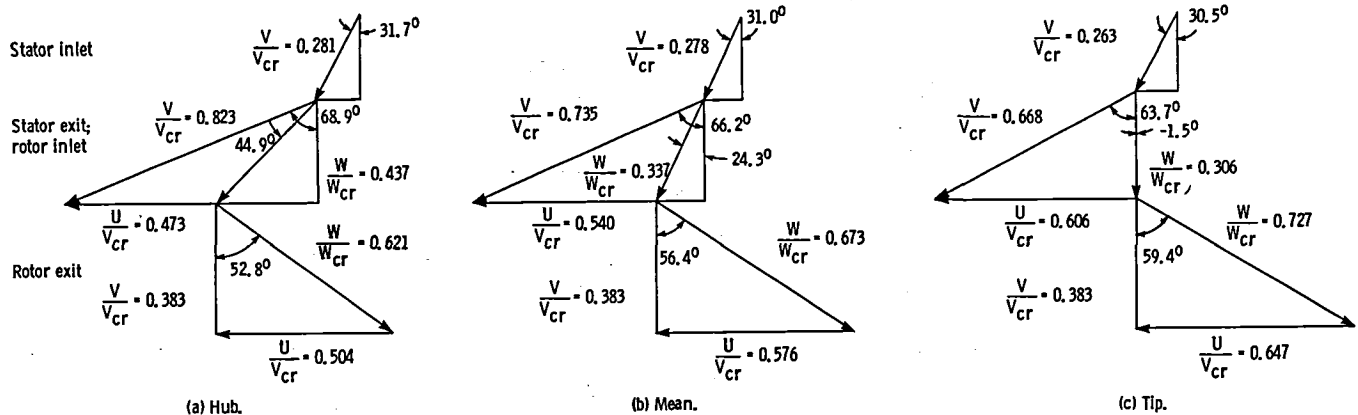


Figure 2. - Free-stream design-point velocity diagrams.

an aerodynamic standpoint to reduce vane loading and to increase aspect ratio.

The stator aerodynamic and geometric parameters are given in table III for the design stator setting angle, and the mean-section vane shape and flow passage are shown in figure 4(a) for stator setting angles of 30.0° , 35.3° (design), and 40.0° . The variation in stator throat area with stator setting angle is shown in figure 4(b). The stator throat area changed from 79.3 percent of the design throat area at a stator setting of 30.0° to 135.6 percent at a stator setting of 45.0° . The axial chord at the design setting angle was chosen to yield a Zweifel loading coefficient of 0.8. Reference 5 assumed that this value of loading corresponded to minimum losses for vane-end clearances of zero. To reduce the chance of rubbing, which is caused by thermal distortion of the spherical end walls and vanes as each vane is rotated on its stem axis, the true chord was kept as short as possible. The stator vane-end clearances were 0.015 centimeter at both hub and tip (total clearance of 1.8 percent of stator passage height). The mean-section solidity c/s was 1.15. This value was somewhat low according to figure 10 of reference 5, which recommends a value of about 1.6. The stator aspect ratio of 0.789 was low enough to result in significant secondary flow and end-wall losses. The design loading diagrams, for the zero vane-end clearance case, at hub, mean, and tip sections are shown in figure 5. These diagrams were calculated with the computer codes of references 6 and 7 (MERIDL and TSONIC). The surface velocity distributions shown in figure 5 are smooth, with an acceptable total diffusion parameter D of 0.395 for the mean section. The acceptable diffusion was the result of the high reaction level in the stator, $R_x = 0.857$, for the mean section (table III). The stator was designed for -9.0° of incidence so that, when the stator was closed for engine control, the incidence was still within the minimum loss region.

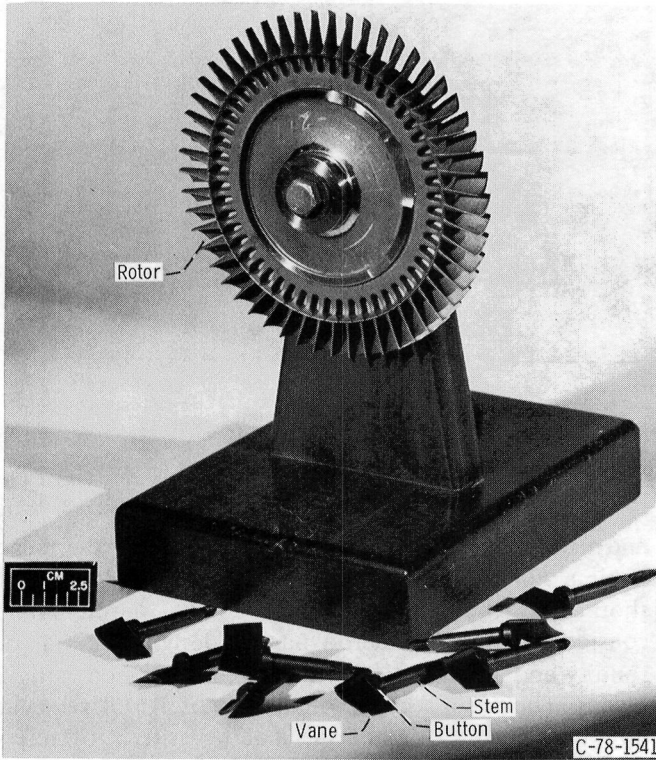
Rotor. - The rotor aerodynamic and geometric parameters are given in table III, and the blading profile

and flow passage are shown in figure 4(a) for the mean section. For manufacturing ease the rotor blade number should be the minimum allowed by aerodynamic considerations. The aerodynamic design criteria of solidity and aspect ratio used resulted in a rotor with 53 blades. The mean-section solidity c/s of 1.613 was near optimum on the basis of the loading criteria of reference 5, and a lower limit on aspect ratio h/c of 1.29 was used to avoid large end-wall-induced losses. Blade loading diagrams were calculated by using MERIDL and TSONIC and are shown in figure 6 for the hub, mean, and tip sections. The blade reaction level was relatively high, and blade surface diffusions were within the design limit of 0.5. The blade incidence at design point was about -5.0° . The design rotor tip clearance was 0.051 centimeter (3 percent of blade height). The rotor tip clearance was recessed into the shroud by using a sharp step in the shroud wall upstream of the rotor. This type of configuration has been found to have lower clearance losses than one where the rotor blade height is reduced and a continuous shroud wall is used (ref. 8).

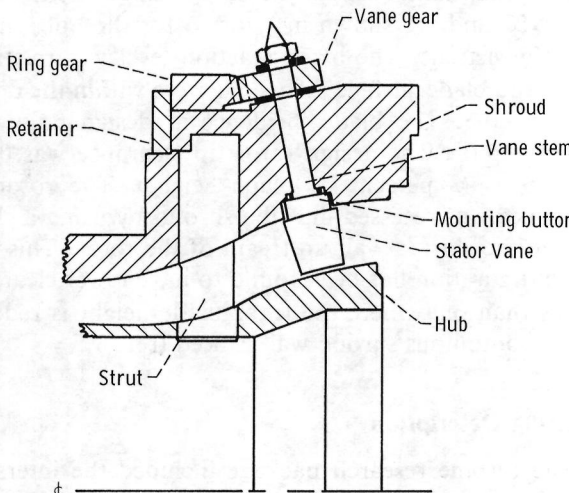
Ducting Description

The turbine research package included the interstage transition duct between the compressor drive turbine exit and the power turbine inlet as well as the exit diffuser, which recovered the power turbine exit kinetic energy and provided a transition into the regenerator. These ducts were included in the turbine flow path so that their interaction effects on turbine blading performance could be included in the performance evaluation. The design procedure for both ducts is described in reference 4.

Interstage transition duct. - The interstage duct provides diffusion of the flow as well as a transition from the smaller diameter compressor turbine to the larger diameter power turbine. The design effort attempted to provide for maximum pressure recovery (static pressure rise divided by inlet dynamic head) within the geometry



(a) Stator vanes and rotor hardware.



(b) Variable-area stator assembly.
Figure 3. - Configuration of stator and rotor.

constraints of inlet and exit annulus areas and overall duct length. An overall diffuser geometry was defined on the basis of the correlation presented in reference 9. This duct was limited to a ratio of length to inlet annulus height $\bar{S}/\Delta R$ of 4.5. The corresponding optimum ratio of exit to inlet area was about 1.89, and the predicted pressure recovery was 0.57. The design area ratio from the compressor turbine exit (station 2) to the power turbine stator inlet (station 3) was 1.88. The hub and

TABLE III. - BLADING GEOMETRIC AND AERODYNAMIC DESIGN PARAMETERS

Parameter	Stator			Rotor		
	Hub	Mean	Tip	Hub	Mean	Tip
Chord, c , cm	1.900	2.151	2.403	1.463	1.311	1.278
Leading-edge radius, cm	0.076	0.089	0.102	0.048	0.038	0.028
Trailing-edge radius, cm	0.025	0.030	0.036	0.030	0.025	0.018
Solidity, c/s	1.16	1.15	1.14	2.053	1.613	1.399
Aspect ratio, h/c	-----	0.789	-----	-----	1.29	-----
Reaction, ^a R_x	0.883	0.857	0.845	0.505	0.771	0.823
Diffusion, ^a D	0.399	0.395	0.377	0.461	0.482	0.325
Clearance, cm (percent of h)	0.015 (0.9)	----- (0.9)	0.015 (0.9)	----- (0.9)	----- (0.9)	0.051 (3.0)

^aStator aerodynamic parameters for design setting angle of 35.3.

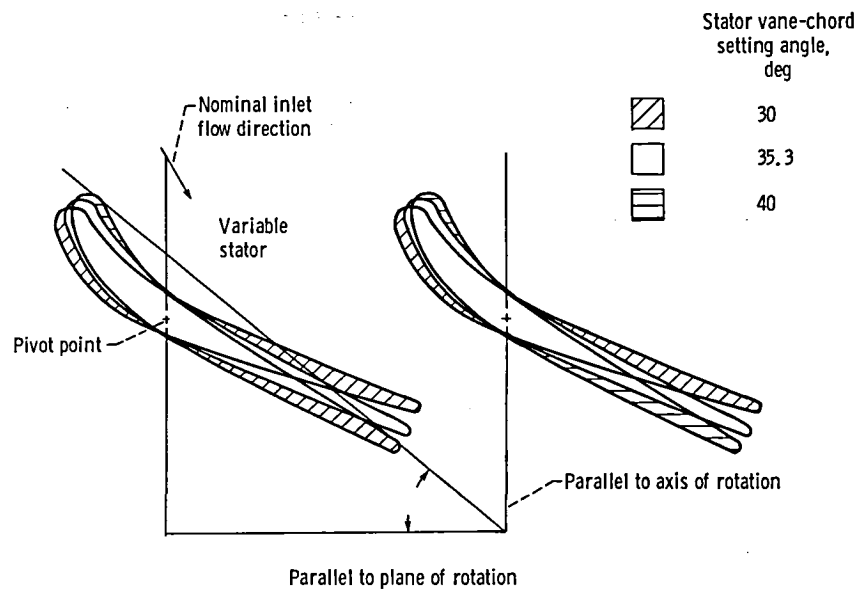
shroud wall contours were developed to provide a gradual increase in wall static pressures by using the MERIDL computer code (ref. 6), an axisymmetric, inviscid analysis. A 2-percent total pressure loss between stations 2 and 3 was assumed.

The centerbody of the duct was supported by three evenly spaced, streamlined struts that were aligned with the calculated flow direction. The total strut flow blockage was 2 percent, and the struts should not have affected duct performance if the alignment was correct. The interstage duct meridional flow path is shown in figure 1. Preswirl vanes were positioned just upstream of the duct inlet (station 2) to provide design swirl into the interstage transition duct.

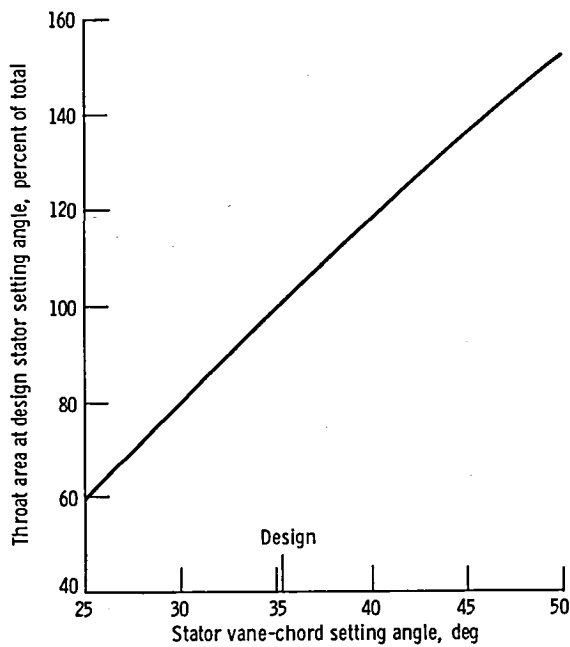
Exit diffuser. - The exit diffuser duct was designed to provide a smooth transition from the power turbine exit (flow primarily axial) to the regenerator plenum inlet (flow primarily radial) and to provide acceptable static pressure recovery for good stage performance. Packaging constraints limited the $\bar{S}/\Delta R$ parameter to 4.3. The optimum area ratio (ref. 9) was 1.85. An area ratio of 1.90 was chosen as the design value. The static pressure recovery was predicted to be 0.58. The flow path surface contours were developed by using the same analysis code as used for the interstage duct design. The meridional flow path is shown in figure 1.

Apparatus

The apparatus consisted of the turbine research package, an airbrake dynamometer to absorb and measure the power output of the turbine, and an inlet and exhaust piping system with flow controls. A schematic of the apparatus is shown in figure 7(a), and the research rig is shown in figure 7(b). Pressurized dry air was used as the working fluid for both the turbine and the airbrake.



(a) Vane and blade shapes and flow passages for mean section.



(b) Variation in stator throat area with stator setting angle.

Figure 4. - Stator and rotor blading geometry.

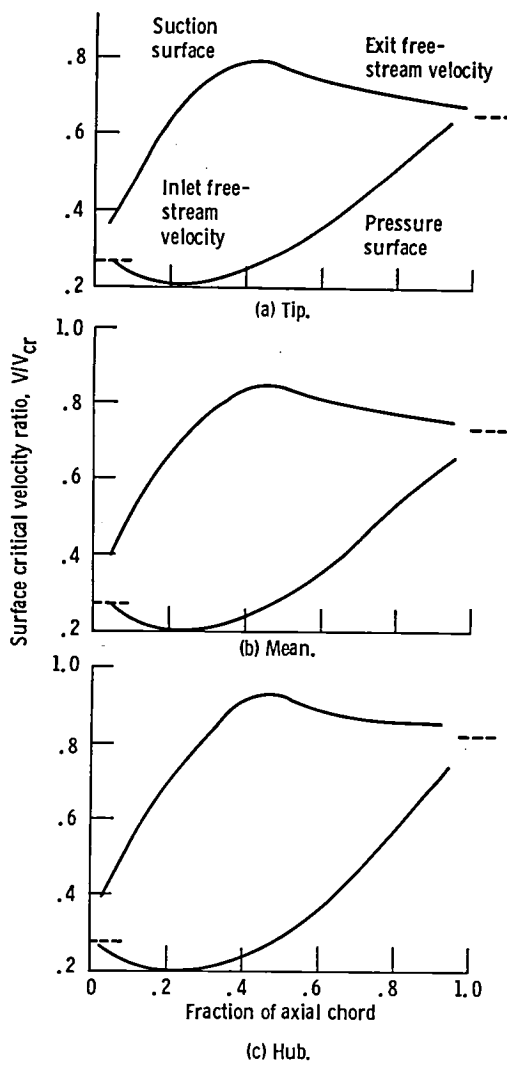


Figure 5. - Design stator vane surface velocities.

Air was piped into the turbine through a filter, an electrical heater, a mass-flow-rate-measuring station (a calibrated flat-plate orifice), and a remotely controlled pressure-regulating valve. The air, after passing through the turbine, was exhausted through a system of piping and a remotely operated valve into the laboratory low-pressure exhaust system.

The airbrake dynamometer was cradle mounted on air bearings for reaction torque measurement. The force on the torque arm was measured with a commercial strain-gage load cell. The rotational speed was measured with a magnetic pickup and a shaft-mounted gear.

Instrumentation

The various turbine performance parameters were determined by measurement of internal temperatures, pressures, and flow angles and by the speed, torque, and

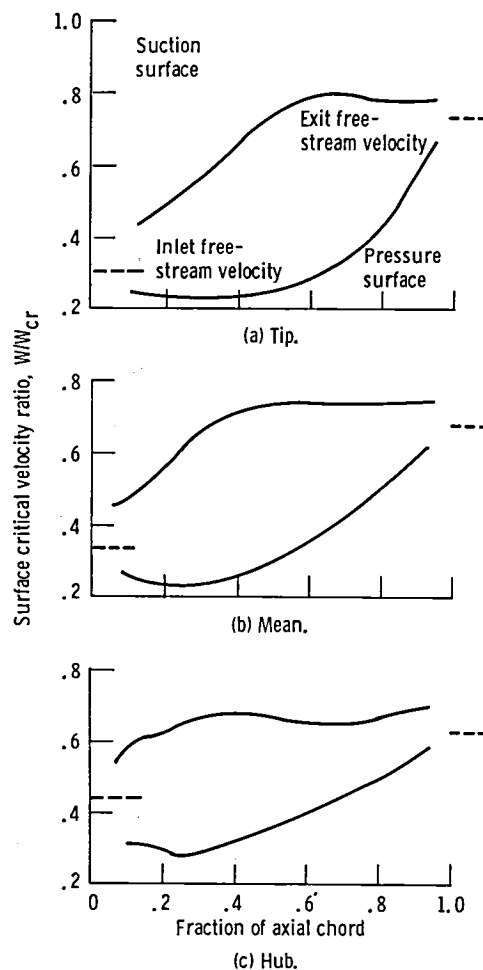


Figure 6. - Design rotor blade surface velocities.

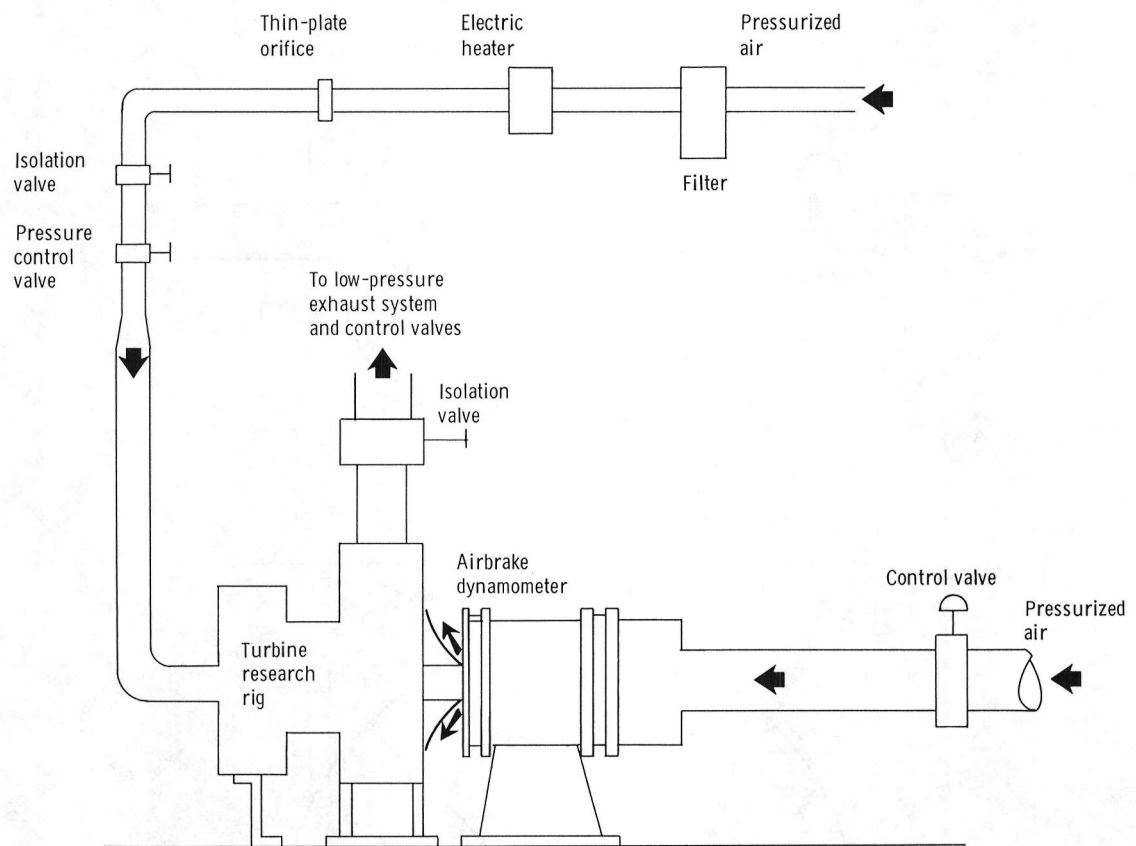
mass flow rate measurements discussed in the section Apparatus. The research turbine flow path and measurement stations are shown in figure 8(a) for the stage performance setup. The turbine was rated on the basis of measurements taken at stations 3, 5, and 7. The type of research instrumentation used at each station is shown in figure 8(b).

Station 1

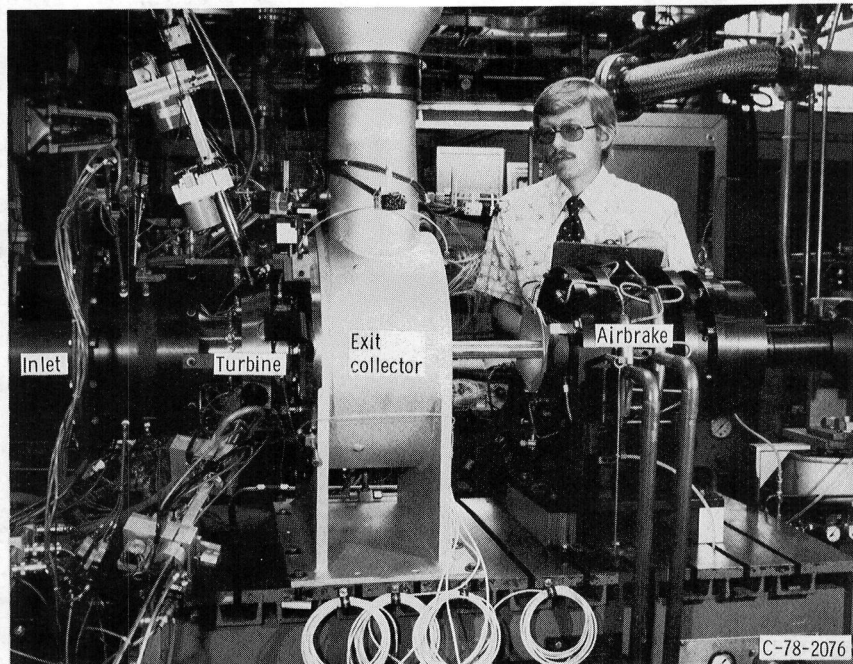
Turbine inlet total temperature was measured with four total temperature rakes positioned as shown in figure 8(b). The inlet plenum static pressure was measured with three static taps located about the circumference of the plenum as shown in figure 8(b). Since the velocity was very low in the inlet plenum, this measured static pressure was near the actual plenum total pressure.

Station 2

As shown in figure 8(a) this station was downstream of the preswirl vanes at the transition duct inlet. Four static



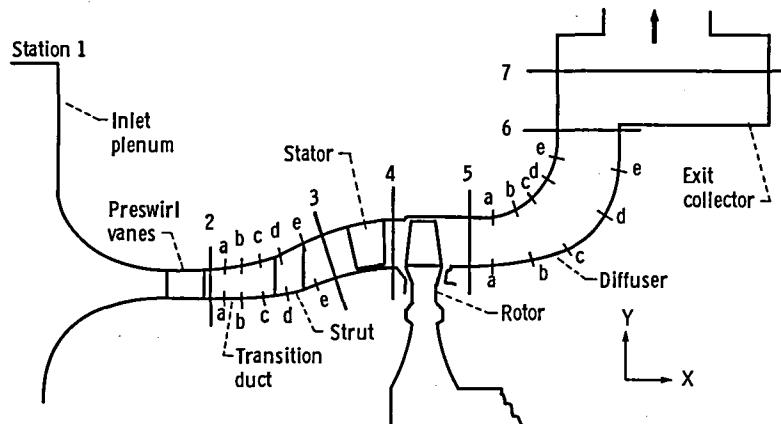
(a) Schematic of piping and test equipment.



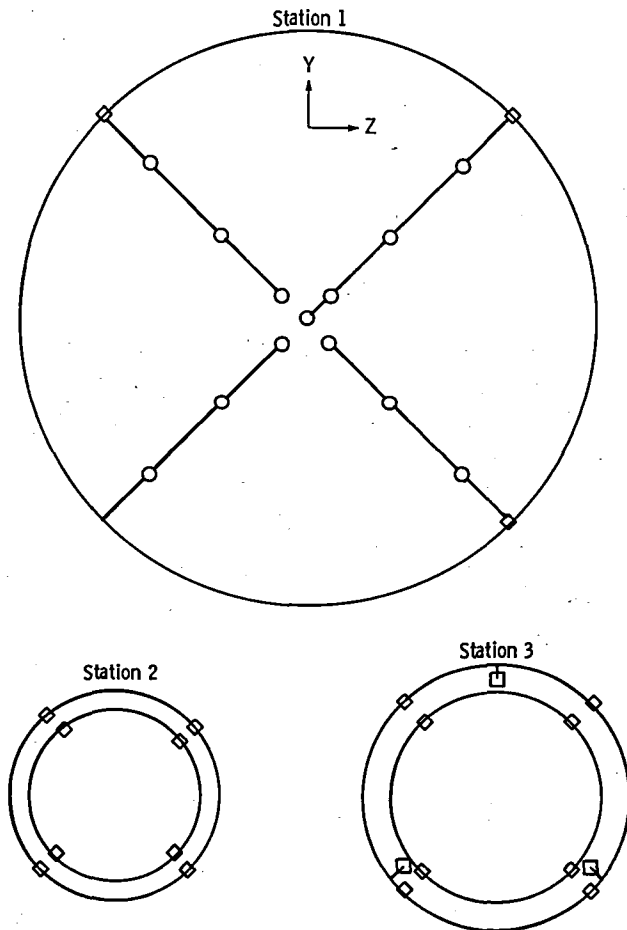
(b) Turbine test apparatus.

Figure 7. - Experimental equipment.

- ◇ Wall static pressure taps
- Survey probe: flow angle, total pressure, and total temperature
- Thermocouple rake

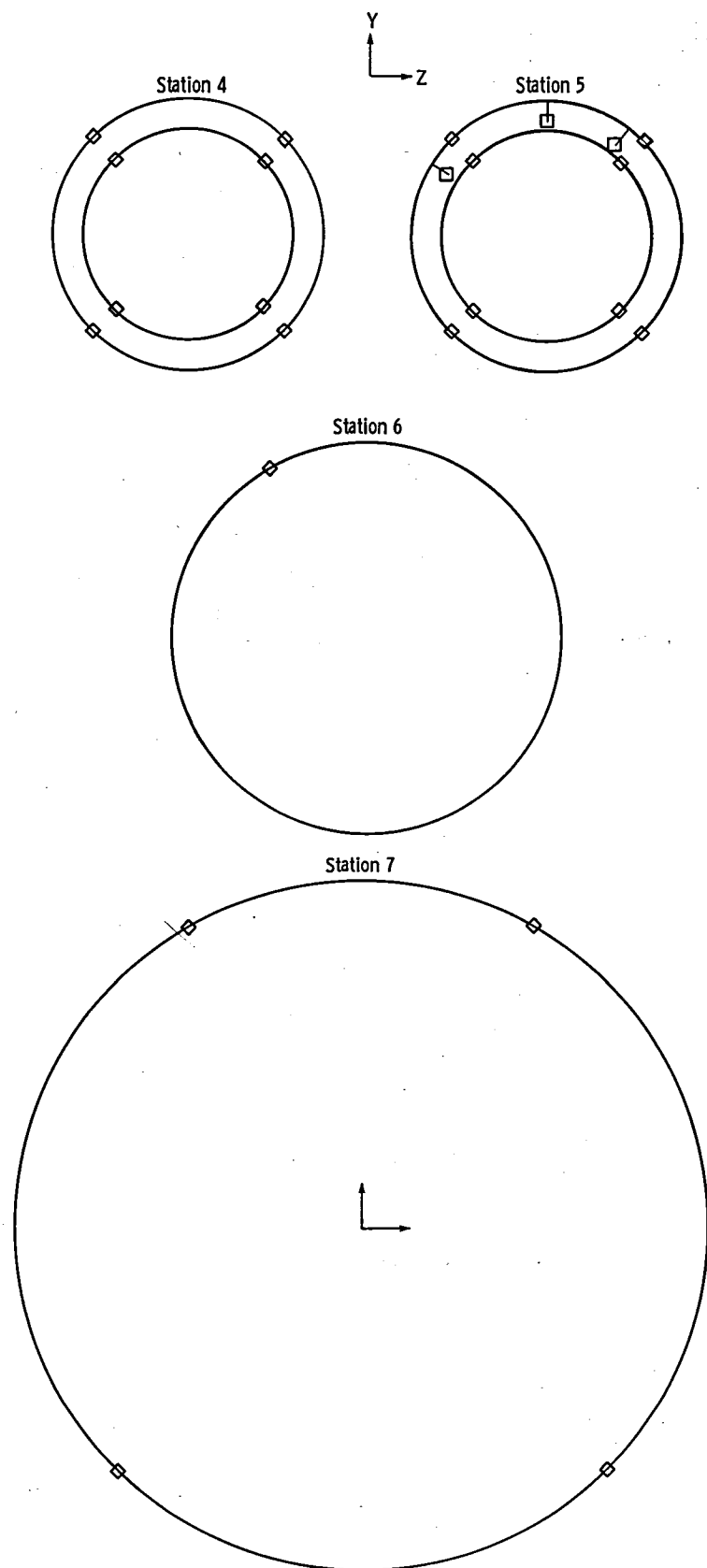


(a) Turbine flowpath and measuring stations.



(b) Research instrumentation.

Figure 8. - Research turbine flowpath and instrumentation.



(b) Concluded.

Figure 8. - Concluded.

taps each on the hub and shroud walls were positioned uniformly about the circumference as shown in figure 8(b). The static taps were positioned circumferentially so that they were not in the preswirl vane wakes. In the transition duct there were two axial rows of static taps, one row each on the hub and shroud walls with five taps total on each wall (labeled a to e in fig. 8(a)). These static taps were evenly spaced axially and were positioned circumferentially so that they were not near the struts.

Station 3

This station was approximately 1/2 stator chord length upstream of the stator inlet. The turbine was rated in part on the basis of measurements taken at this inlet station. Eight static pressure taps, four each on the hub and shroud walls, were uniformly spaced around the circumference as shown in figure 8(b). The radial variations in total temperature, total pressure, and flow angle at the stator inlet were measured with three self-aligning probes equally spaced around the circumference as shown in figure 8(b). The probe-actuator assembly is shown in figure 9(a), and a close up of the probe sensing

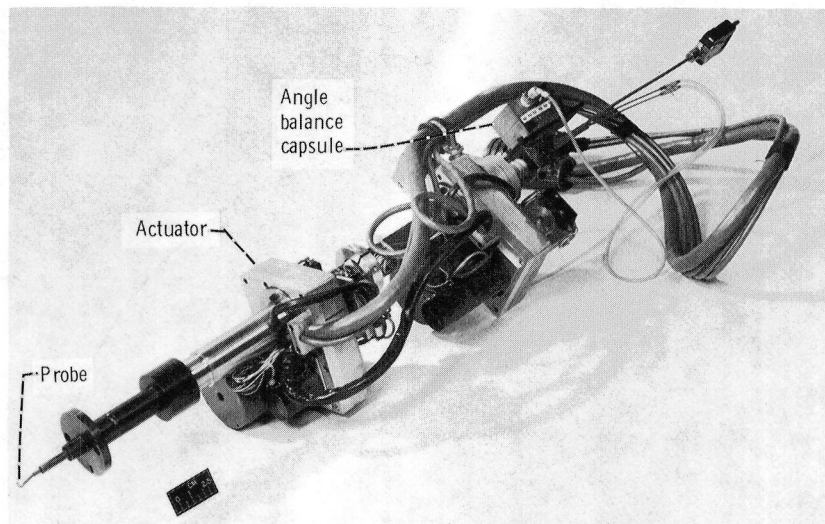
elements is shown in figure 9(b). Data were taken with the three probes at 11 radial positions from hub to shroud.

Station 4

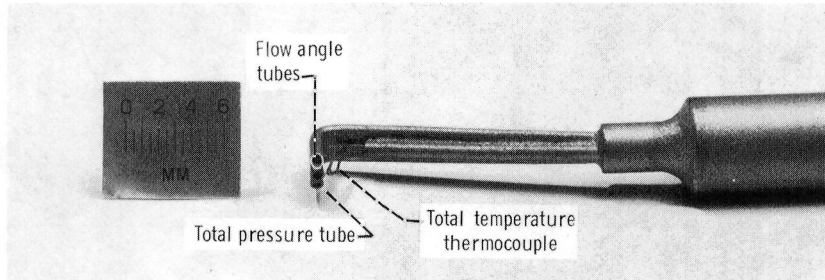
The static pressure at station 4 was measured by eight static taps, four each on the hub and shroud walls, evenly spaced around the circumference as shown in figure 8(b). Stator exit fluid torque was measured as a reaction torque on a stationary paddlewheel rotor attached to the airbrake load cell via the turbine shaft as shown in figure 10. All instrumentation upstream of the rotor was retained for these tests. The instrumentation at stations 5, 6, and 7 was not in use for the stator performance tests.

Station 5

Measurements were taken at station 5 about one rotor-mean-section axial chord length downstream from the rotor trailing edge. Static pressure was measured with eight taps, four each on the hub and shroud walls, evenly spaced around the circumference as shown in figure 8(b). The radial variations in total temperature, total pressure,



(a) Actuator, balance capsule, and probe assembly.



(b) Total pressure, total temperature and flow angle probe.

Figure 9. - Survey probe instrumentation.

and flow angle at the rotor exit were measured with the three self-aligning probes (fig. 9) discussed previously. Because of space limitations in the test cell the probes were confined to a sector of 100° at the top of the test rig (fig. 8(b)).

Station 6

The static pressure variations through the exit diffuser were measured with 12 static taps, six each on the hub and shroud walls (fig. 8(a)). The taps were aligned in the axial direction at the circumferential position indicated for station 6 in figure 8(b).

Station 7

The stage exit static pressure was measured in the exit collector by eight static taps, four each on the hub-side and shroud-side bulkheads. The taps were located circumferentially as shown in figure 8(b), with the two taps at each circumferential position tied together to give one pressure reading.

Procedure

Stage Performance

Data were taken at nominal stator inlet total-state conditions of 320 K and 0.409 atmosphere. These inlet conditions allow design-point operation at the same Reynolds number as that encountered in engine operation. Data were obtained for ratios of stator inlet total pressure to rotor exit static pressure from 1.18 to 3.50, for speeds from 0 to 130 percent of design, and for stator throat areas from 79.3 to 135.6 percent of design (stator vane-chord setting angles of 30°, 35.3°, 40°, and 45°).

Friction torque of the bearings, the seals, the coupling windage, and the rotor disk windage was obtained by measuring the amount of torque required to rotate the shaft and rotor disk without blades over the range of speeds encountered in this investigation. The turbine cavity was evacuated to a pressure of 3.31 N/cm², which was approximately the pressure level in the rotor disk cavity during stage tests. On the basis of test inlet conditions the friction torque at design speed was 0.21 N-m, or about 18 percent of the turbine aerodynamic torque at design point. Friction torque was added to the dynamometer torque to obtain the turbine aerodynamic torque.

The turbine total and static efficiencies are based on pressure measurements taken at stations 3, 5, and 7 as well as on the measurements of temperature, speed, torque, and mass flow rate. The turbine inlet (station 3) total pressure P'_3 was determined from a correlation of mass-averaged total pressure (calculated from inlet radial surveys) as a function of flow rate w and inlet static pressure P_3 (see the section **Instrumentation**). This was done to account for the large radial gradients in total pressure and flow angle at the turbine stator inlet. The overall pressure at the rotor exit (station 5) was calculated from the mass flow rate, the static pressure, the total temperature, and the flow angle with the following equation:

$$P'_5 = P_5 \left\{ \frac{1}{2} + \frac{1}{2} \left[1 + \frac{2R(\gamma-1)}{\gamma} \times \left(\frac{w\sqrt{T_5}}{P_5 A_5 \cos \alpha_5} \right)^2 \right]^{1/2} \right\}^{\gamma/(\gamma-1)}$$

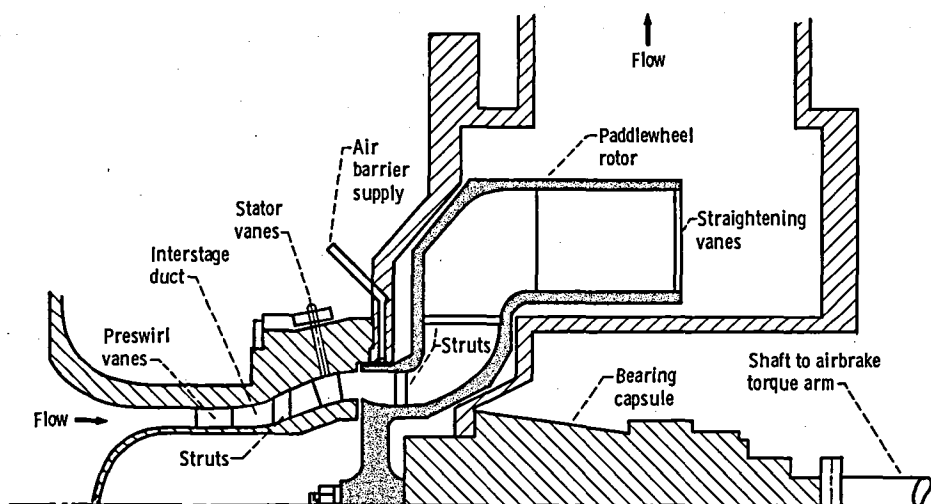


Figure 10. - Schematic of paddlewheel setup for stator performance tests.

Stator Performance

Data were taken at nominal stator inlet total-state conditions of 295 K and 0.409 atmosphere. Data were obtained for ratios of stator exit static pressure to stator inlet total pressure from 0.380 to 0.921 and for stator throat areas from 79.3 to 135.6 percent of design.

Stator performance was determined from measurements of pressure, temperature, exit fluid torque, and mass flow rate. The stator inlet total pressure was determined from the same correlation of turbine inlet total pressure as that discussed in the section Stage Performance. Stator exit fluid torque was measured with the paddlewheel rotor configuration shown in figure 10 and described in the section Instrumentation. An air barrier was used to equalize the pressures between the stator exit shroud and the shroud-paddlewheel rotor clearance gap to prevent flow leakage around the paddlewheel rotor.

Results and Discussion

Experimentally determined performance data are presented for the interstage transition duct and the power turbine stator as well as for the turbine stage and the exit diffuser. Interstage duct performance and stator performance were determined at nominal inlet conditions of 295 K and 0.409 atmosphere. The results of duct wall static pressure measurements and duct exit radial surveys are discussed. Stator performance was determined with the paddlewheel rotor configuration discussed in the section Instrumentation, and the results are presented in terms of mass flow rate and stator exit moment of momentum. Power turbine stage performance was determined at nominal inlet conditions of 320 K and 0.409 atmosphere. The results are presented for stator vane-chord setting angles of 30°, 35.3°, 40°, and 45° in terms of mass flow rate, torque, speed, power, and efficiency. The radial variations in rotor exit flow conditions are presented for each stator setting angle. The exit diffuser performance at design conditions is also presented.

Interstage Duct Performance

The experimentally obtained hub and shroud static pressure variations through the interstage duct are presented in figure 11 for two values of turbine equivalent mass flow rate (0.611 and 0.558 kg/s). The experimental values of static pressure have been nondimensionalized with a calculated value of station 2 total pressure P_2' . This value includes the mixing loss of the preswirl vane wakes. One mass flow rate was 1.6 percent higher and the other was 7.2 percent lower than the design equivalent value for cold hardware

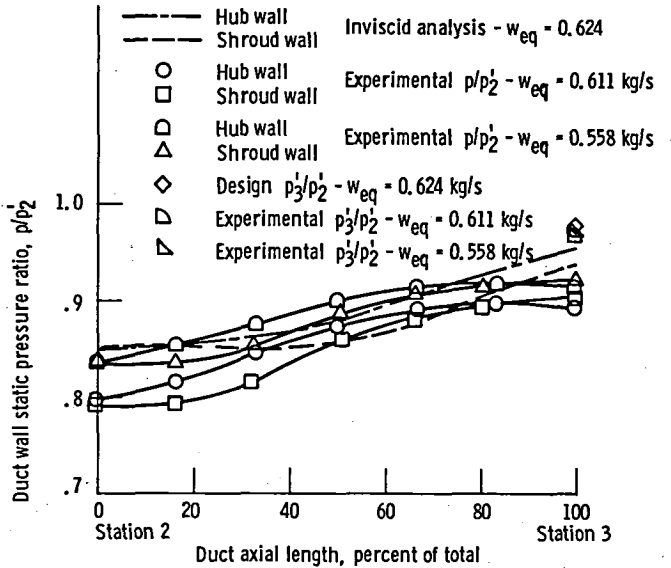


Figure 11. - Analytical and experimental variations in wall static pressures through interstage transition duct.

dimensions. Also shown in figure 11 is the design variation of wall static pressure that was calculated by assuming inviscid, axisymmetric flow and a 2-percent loss in total pressure through the duct. That the static pressure ratios for both flow rates were lower than the design values at the duct inlet indicates that the flow Mach number was higher than design for both cases. This results from the preswirl vanes' 11.4 percent trailing-edge blockage. The total aerodynamic blockage including that of the end-wall boundary layers was thus about 13 percent, whereas the inviscid analysis assumed the flow to be uniform with no blockage. Furthermore the rate of actual static pressure recovery was greater than shown in the inviscid analysis in the front half of the duct and less in the rear half of the duct. Unpublished interstage duct data from the compressor drive turbine investigation also indicate these pressure recovery trends. These comparisons reveal the difficulty of using an inviscid flow code for modeling the flow in this interstage duct. The experimentally obtained pressure recovery coefficients were 0.559 and 0.552 for the high- and low-flow cases, respectively. The design value of pressure recovery was 0.570.

Surveys of total pressure and flow angle were taken at the exit of the interstage duct (station 3) to determine the best method for obtaining a single representative value for turbine inlet total pressure for use in subsequent turbine stage efficiency calculations. Three typical surveys (at turbine equivalent flow rates of 0.938, 1.06, and 1.203 times the equivalent design value with cold dimensions) are presented in figure 12, which plots local values of total pressure, flow angle, and vane incidence angle as a function of percent of passage height. The

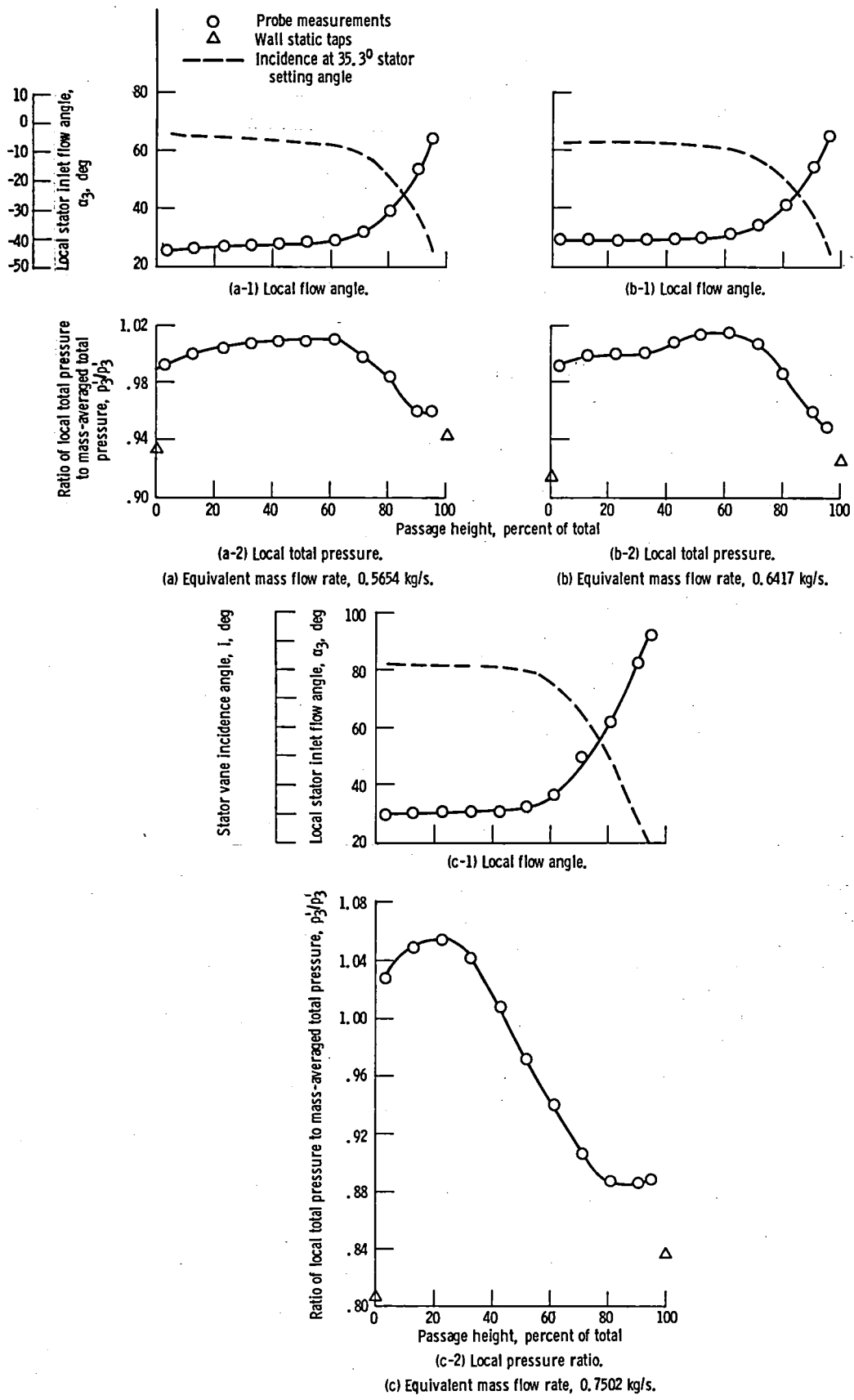


Figure 12. - Radial variation of stator inlet flow angle, incidence angle, and total pressure.

values of local total pressure have been nondimensionalized by dividing by the mass-averaged value of total pressure at station 3. For the two lower values of flow rate (figs. 12(a) and (b)), the inlet profiles are similar and indicate that from about 60 percent of passage height out to near the shroud (95 percent) the flow angle and total pressure changed drastically from the trend that was observed for the other part of the passage. Specifically (fig. 12(b)) the flow angle increased from about 30° to 66° and the total pressure ratio decreased from a peak of about 1.015 to about 0.95. The combined effects of decreasing total pressure and increasing flow angle were that the mass flow rate per unit height decreased rapidly from 60 percent of passage height out to the shroud. For the highest value of mass flow rate (fig. 12(c)) the distortion of the inlet profile was much greater. The increase in the flow angle began at 50 percent of the passage height and increased to 92° at 95 percent of the passage height. The total pressure ratio peaked at a value 1.055 times the mass-averaged value near 25 percent of the passage height and decreased almost linearly to 0.886 at about 85 percent of the passage height. These trends indicate rapidly decreasing mass flow rate per unit height from about 25 percent to 80 percent of the passage height as well as high losses in the region of the shroud wall. It is probable that flow separation existed at the survey plane (station 3) for the highest flow rate. Also there was overexpansion of the flow through the stator near the hub because the inlet total pressure there was 5.5 percent greater than the mass-averaged value.

The incidence angle for the design vane-chord setting angle of 35.3° is also shown in figure 12. For a setting angle of 30° the curve should be offset by adding 5.3° to the incidence angle. For a setting angle of 45° the curve should be offset by subtracting 9.7° from the incidence angle. For the design setting angle, high negative incidence angles occurred in the region near the shroud. With these large variations in flow angle, errors were induced by using a limited sampling of flow angle to calculate a single representative value of turbine inlet total pressure from the equation presented in the section **Procedure**. The single representative value for total pressure was obtained instead by making a number of surveys of total pressure and flow angle covering the range of mass flow rates in this investigation. These survey results were mass averaged, and the total pressure was then nondimensionalized by the static pressure P_3 and plotted against a corrected mass flow rate for use in the stage performance evaluation.

Stator Performance

The measured values of equivalent mass flow rate w_{eq} and stator exit total moment of momentum $rV_{u,4}$ are

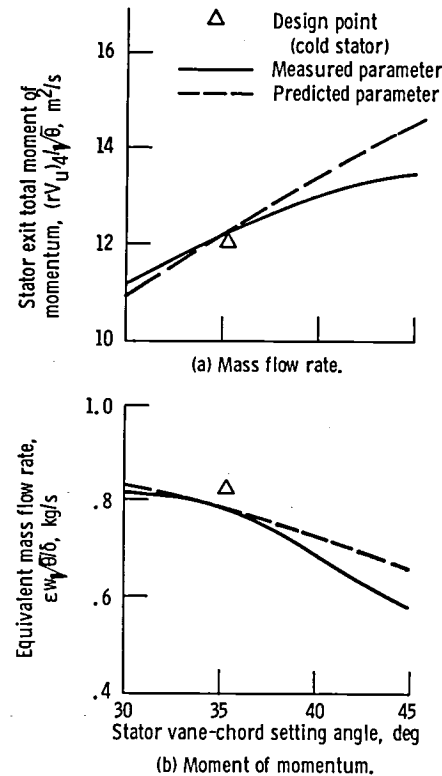


Figure 13. - Variation of stator mass flow rate and exit momentum with stator setting angle at design stator pressure ratio P_4/P_3 of 0.685.

presented in figure 13 as functions of vane-chord setting angle for operation at the equivalent design value of the ratio of stator exit static pressure to stator inlet total pressure P_4/P_3 of 0.685. Increasing the stator setting angle increased the vane throat area. Figure 13 shows that at the design setting angle, 35.3° , the equivalent mass flow rate was 0.624 kg/s and the stator exit total moment of momentum was $13.81 \text{ m}^2/\text{s}$. These values were 3.7 percent higher and 3.1 percent lower than their respective equivalent design values of 0.6015 kg/s and $14.25 \text{ m}^2/\text{s}$ for cold dimensions. The measured stator throat area at the design setting angle was 1.2 percent less than design intent for cold dimensions. If the cold stator throat area had been as designed, the measured mass flow rate would be 4.9 percent greater than the design value.

The measured results of mass flow rate greater than design and stator exit moment of momentum less than design are manifestations of vane-end clearance leakage (ref. 10). The measured stator inlet flow distortion is also expected to affect these two parameters. In the regions where the local inlet total pressure is less than the mass-averaged value, the local values of expansion ratio, mass flow rate, and tangential velocity will tend to be less than design. The velocity gradients resulting from this inlet flow distortion, when combined with the forces needed to

satisfy equilibrium in the meridional and blade-to-blade planes, will result in significant secondary flows within the vane passage. Secondary flows are reflected in overturning in regions of low velocity (near the end walls) and undeturning in regions of high velocity (at midspan or in the core flow).

The effect of secondary flows on mass flow rate and stator exit moment of momentum cannot be quantified by using current analytical methods. However, with the assumptions that the effects of vane-end clearance and inlet flow distortion on losses and leakage are unchanged as the stator is opened and closed from the design setting angle, the mass flow rate and the moment of momentum at other setting angles can be predicted from the design variation of stator exit flow angle. The quantities adjusted for the variation of flow angle with setting angle were the measured values at the design setting angle. The predicted trends in mass flow rate and moment of momentum with stator setting angle obtained in this manner can be compared with the measured trends to obtain some insight into the relative significance of vane-end clearance leakage and inlet flow distortion.

The predicted trends in mass flow rate and moment of momentum with setting angle are shown in figure 13 by the dashed lines. The predicted mass flow curve (fig. 13(a)) intersects the measured curve at the 35.3° setting angle, as expected; underestimates the flow at the 30° setting angle; and greatly overestimates the flow at the 40° and 45° setting angles. The predicted total-moment-of-momentum curve (fig. 13(b)) is tangent to the measured curve at the 35.3° setting angle but overestimates the moment of momentum for all other stator setting angles.

The differences between predicted and measured curves should indicate the effects of vane-end clearances and inlet flow distortion on stator performance. For the 30° setting angle the effects of vane-end clearance leakage should make the measured value of mass flow higher than the predicted value and the measured value of moment of momentum lower than the predicted value. This results from the fact that the leakage flow area at the 35.3° setting angle was smaller relative to the stator throat area than it was at the 30° setting angle. This trend did occur as shown in figure 13.

Since the inlet flow distortion did not significantly change between the 30° and 35.3° setting angles (figs. 12(a) and (b)), it can be concluded that the differences between the predicted and measured values at the 30° setting angle were due primarily to vane-end clearance leakage effects. For the 40° and 45° setting angles the effects of reduced vane loading on end clearance leakage should make the measured values of mass flow rate lower than the predicted values and the measured values of moment of momentum higher than the predicted values. The measured-mass-flow-rate curve in figure 13(a) shows

this difference between predicted and measured values, which becomes quite large at the 45° setting angle. The expected differences between predicted and measured values of moment of momentum did not occur. The additional effects of the inlet flow distortion may be altering the stator performance characteristics in this high-flow regime.

Figures 12(b) and (c) show the large changes in inlet flow distortion that occurred between the design flow rate and the high flow rates corresponding to 40° and 45° setting angles. The effects of the inlet flow distortion observed herein on the comparison of measured and predicted values of mass flow rate and moment of momentum were to decrease both the measured values relative to the predicted values. This trend can be rationalized by recalling that the inlet distortion would cause overexpansion and high mass flow rate in the hub region and underexpansion and low flow rate in the shroud region. Even though the mass-averaged expansion ratio was the same as one without distortion in the inlet flow, the overexpansion and high flow in the hub region did not compensate for the underexpansion and low flow in the shroud region. This occurred because the annulus area per unit height below the mean radius was less than the annulus area per unit height above the mean radius. Thus the net result of the change in distortion between the design setting angle and higher values of setting angle was reduced mass flow rate per unit area. By similar deduction the overexpansion occurred in a region of lower radius and the underexpansion occurred in a region of higher radius. Thus the moments of momentum of the over- and underexpanded flow added up to a measured value of total moment of momentum that was lower than the predicted value. Therefore the differences between predicted and measured values at the high stator setting angles were due primarily to the inlet flow distortion effects. Although this exercise did not separate and quantify the effects due to vane-end clearance leakage and inlet flow distortion, it did show the significance of these effects of the power turbine stator performance.

Stage Performance

Stage mass flow rate.—The variation in stage equivalent mass flow rate with the ratio of stator inlet total pressure to rotor exit static pressure P_3/P_5 for lines of constant equivalent speed is shown in figure 14 at stator setting angles of 30°, 35.3°, 40°, and 45°. Stage mass flow rate differed from the stator mass flow rate discussed earlier in that stage flow rate was correlated with stage pressure ratio and rotor speed whereas stator flow rate was correlated with the stator pressure ratio. At the smallest stator area (30° setting angle) shown in figure 14(a) the stator was choked at stage pressure ratios greater than about 2.5. At the larger stator areas the rotor

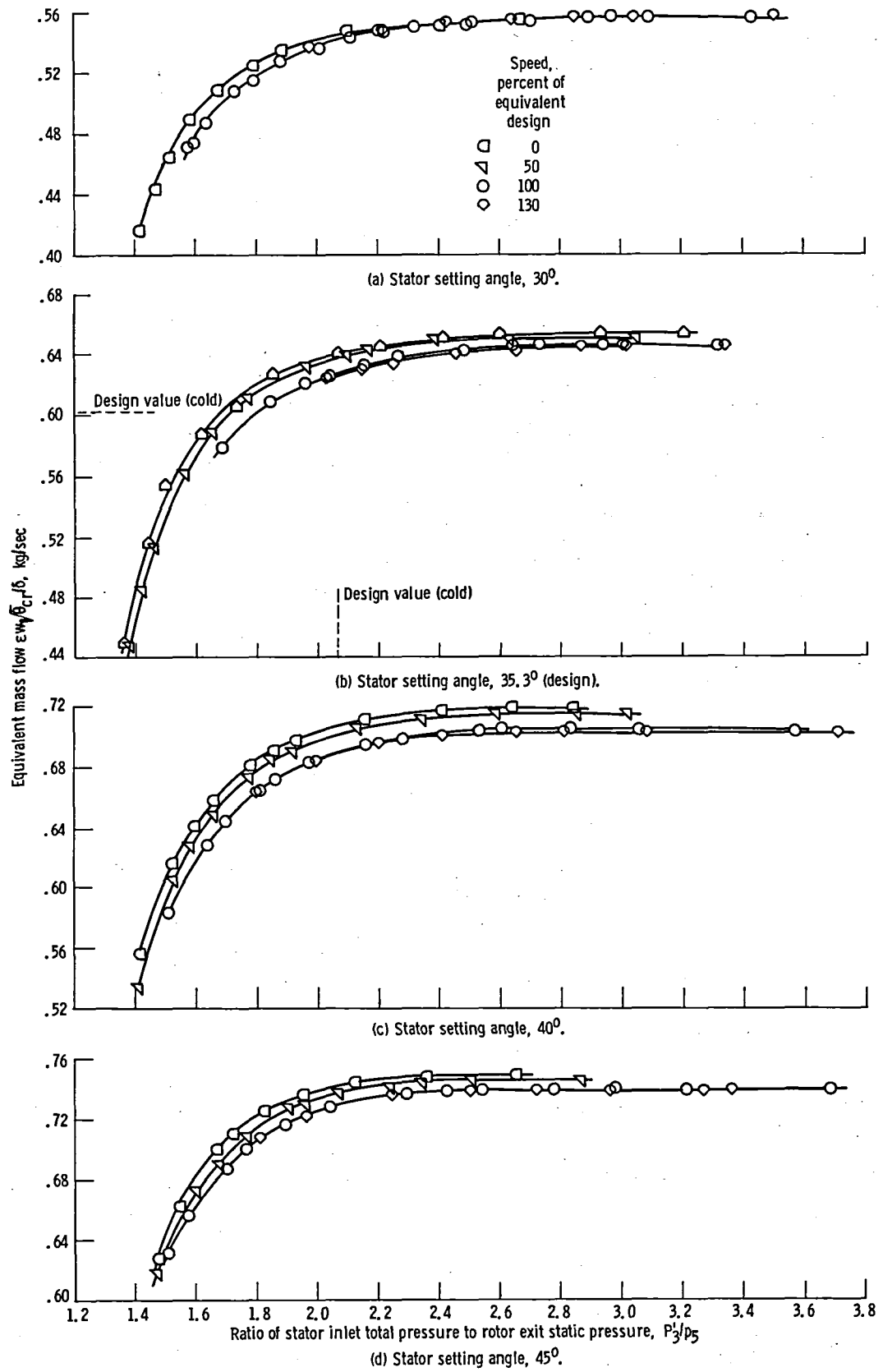


Figure 14. - Variation of mass flow with pressure ratio and speed over range of setting angles.

choked before the stator at most speeds as indicated by the differing values of flow rate for each speed line at the high-pressure ratios in figures 14(b), (c), and (d).

The stage mass flow rate variation for the design stator setting angle of 35.3° is shown in figure 14(b). At equivalent design values of speed and stage pressure ratio (P'_3/P'_5 of 1.867), the measured equivalent mass flow rate was 0.6277 kg/s, which was 4.36 percent greater than the design value for cold hardware dimensions. The measured value was 0.6 percent greater than the measured value of 0.624 kg/s for the design ratio of stator exit static pressure to stator inlet total pressure P'_4/P'_3 of 0.685. This difference is due to the fact that at design stage pressure ratio the stator was slightly overexpanded with a stator pressure ratio of 0.664. This overexpansion implied a mismatch between stator and rotor throat area. The rotor throat area was measured to be 4.3 percent less than "cold" design intent. A rotor throat area 4.3 percent small combined with a stator throat area 1.2 percent small indicated a mismatch that should cause underexpansion of the stator at design stage pressure ratio. However, the large rotor tip clearance, 3 percent of passage height, and its associated leakage effects resulted in a larger effective rotor throat area and thus a slight stator overexpansion.

Stage torque output. — The variation in turbine torque output with stage pressure ratio P'_3/P'_5 for lines of constant equivalent speed is shown in figure 15 at stator setting angles of 30° , 35.3° , 40° , and 45° . Torque increased with increasing pressure ratio and decreasing speed for all stator setting angles. At the design setting angle of 35.3° (fig. 15(b)) the zero-speed torque curve is also shown.

At design equivalent values of speed and a stage pressure ratio P'_3/P'_5 of 1.867, the measured equivalent torque was 7.97 N-m at the design setting angle (fig. 15(b)). This torque value was 7.0 percent less than the design equivalent value for cold hardware dimensions. The combination of a torque value 7.0 percent less than design with a mass flow rate 4.35 percent greater than design resulted in the equivalent specific work being 11.35 percent less than design and the static efficiency, $\eta_{3.5}$, being 0.084 less than the design value of 0.741. The zero-speed equivalent torque (fig. 15(b)) at the design stage pressure ratio of 1.867 was 17.65 N-m, which was 2.21 times the torque at equivalent design speed. The trend of increasing torque with increasing pressure ratio shown in figure 15 indicates limit loading was not reached for the range of pressure ratios investigated.

Turbine efficiency. — Performance maps were developed by crossplotting mass flow rate and torque as functions of speed and pressure ratio. Equivalent power was calculated with values obtained from these data plots and presented as a function of the equivalent mass flow-speed parameter for each of the four stator setting

angles tested. Lines of constant pressure ratio and constant efficiency were superimposed on the plots. Turbine efficiency was defined as the ratio of actual specific work to ideal specific work. Ideal work values were calculated from ratios between the stator inlet total pressure and the rotor exit total pressure P'_3/P'_5 , the rotor exit static pressure P'_3/P'_5 , and the exit collector static pressure P'_3/P'_7 . The operating point corresponding to design equivalent values of rotative speed and power for cold dimensions is shown on each map.

The performance maps based on rotor exit total state conditions are shown for stator setting angles of 30° , 35.3° , 40° , and 45° in figure 16. A peak total efficiency $\eta_{3.5}$ of 0.76 was measured at both 30° and 35.3° in the high-speed, high-pressure-ratio regime. At the operating point corresponding to design equivalent values of speed and power, a total efficiency of about 0.75 was obtained at a setting angle of 35.3° (fig. 16(b)). The total efficiency at this operating condition was reduced by 0.01 when the stator setting angle was reduced to 30° (fig. 16(a)) and was reduced by about 0.02 and 0.06 when the stator setting angle was increased to 40° and 45° , respectively (figs. 16(c) and (d)). The efficiency lost by reducing the setting angle to 30° is attributed to the reduction in rotor reaction and increased stator vane-end clearance losses. The efficiency lost by increasing stator setting angle to 40° and 45° was due primarily to the increased stator inlet flow distortion as mass flow rate was increased, as previously discussed in the section **Stator Performance**. The total efficiency measured at the design equivalent operating point (fig. 16(b)) was 0.10 less than the design value of 0.85. A substantial part of this difference was probably due to the inlet flow distortion. Other effects that may contribute to this difference include vane-end clearance leakage, low stator aspect ratio, the relatively low turbine Reynolds number, and the combined effects of large rotor tip clearance and high reaction.

The performance maps based on rotor exit static conditions are shown for stator setting angles of 30° , 35.3° , 40° , and 45° in figure 17. A peak static efficiency $\eta_{3.5}$ of 0.67 was measured at a setting angle of 30° (fig. 17(a)) near the design equivalent power. This peak occurred at speeds and pressure ratios higher than design because at design values of speed and power the rotor incidence was high. Increasing the speed and pressure ratio reduced rotor incidence and increased rotor reaction, both of which improved turbine efficiency. The static efficiencies at design equivalent values of speed and power were about 0.66, 0.65, 0.62, and 0.57 for stator setting angles of 30° , 35.3° , 40° , and 45° , respectively. The design static efficiency at the 35.3° setting angle was 0.74, or about 0.09 greater than the measured value.

The performance maps based on exit collector static pressure are shown for stator setting angles of 30° , 35.3° , 40° , and 45° in figure 18. The peak overall stage

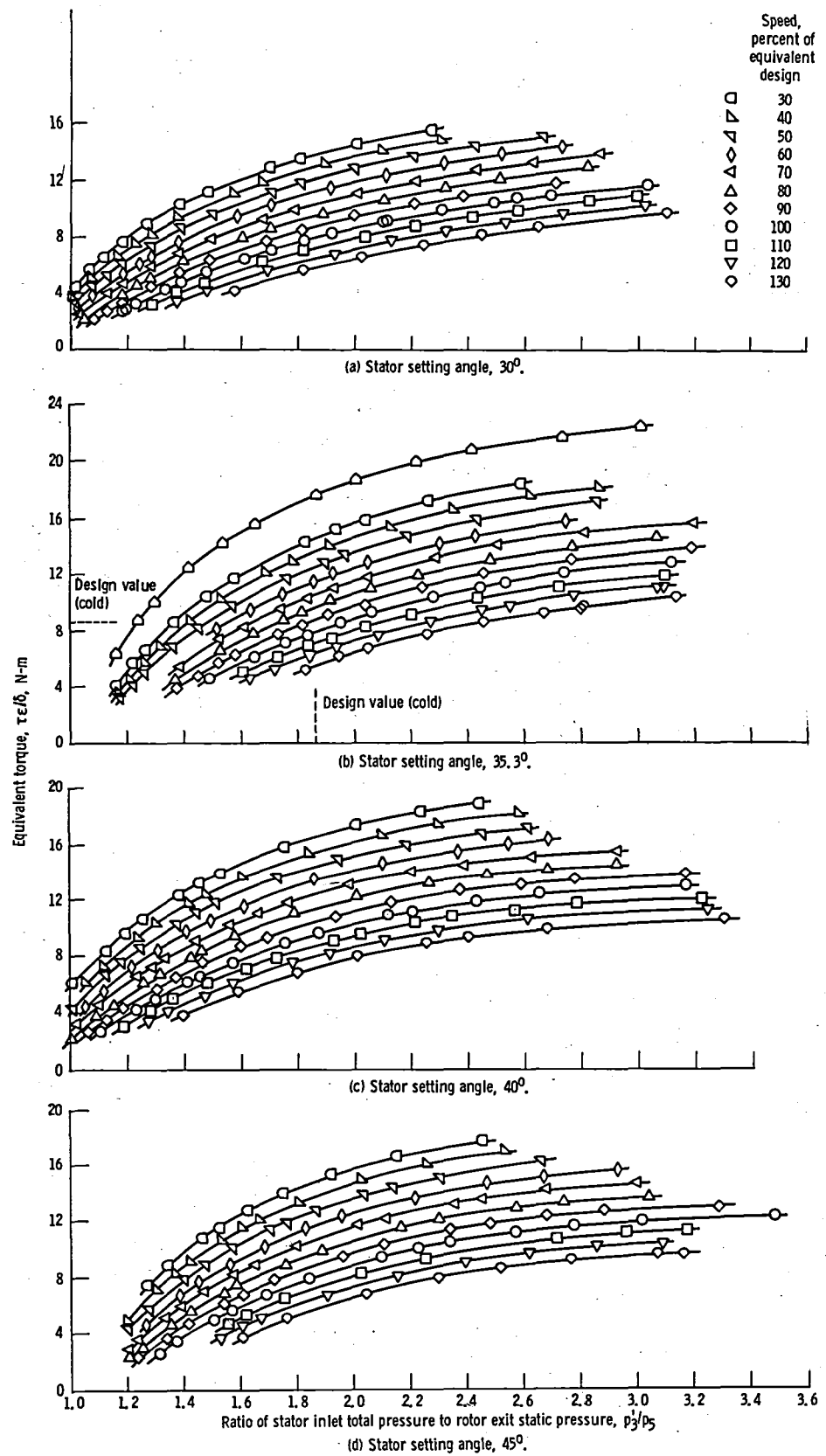


Figure 15. - Variation of torque with pressure ratio and speed over range of setting angles.

——— Speed, percent of equivalent design
 - - - Ratio of equivalent inlet total pressure to
 rotor exit total pressure, p_3/p_5
 - - - Total efficiency, η'_{3-5}
 ● Equivalent design values of speed and power

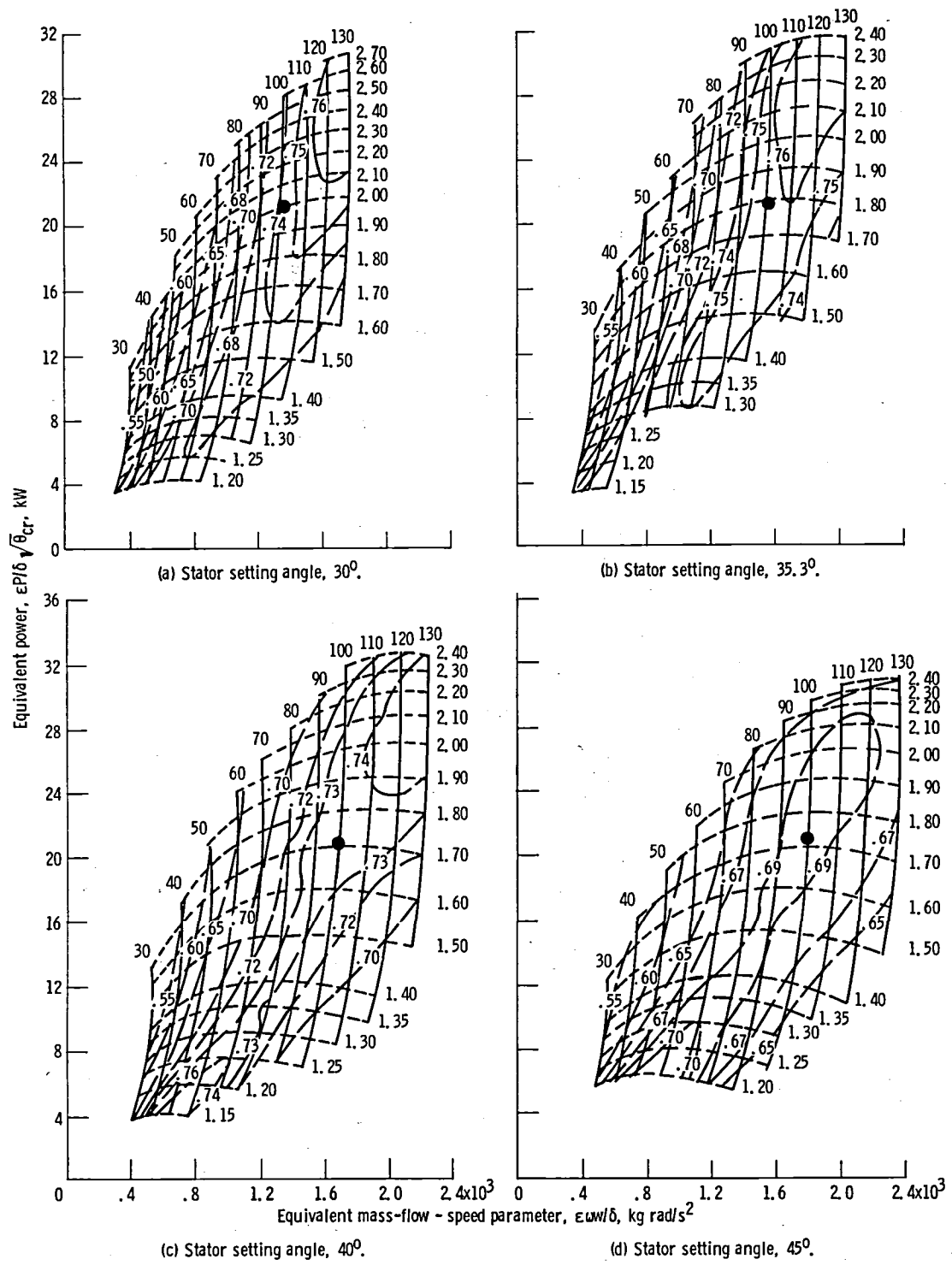


Figure 16. - Turbine performance maps based on rotor exit total state conditions.

— Speed, percent of equivalent design
 - - - Ratio of equivalent inlet total pressure to rotor
 exit static pressure, p_3/p_5
 — Static efficiency, η_{3-5}
 ● Equivalent design values of speed and power

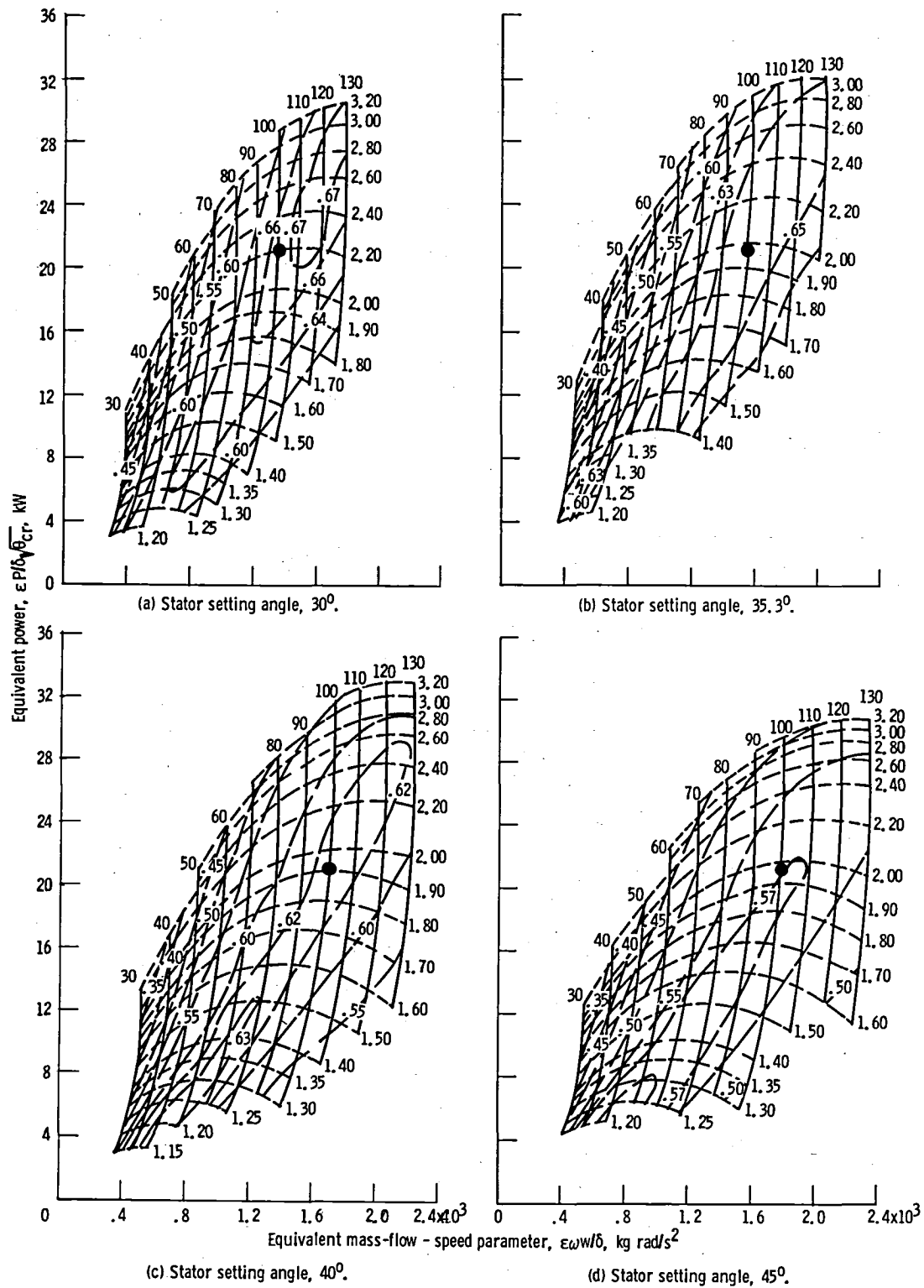


Figure 17. - Turbine performance maps based on rotor exit static conditions.

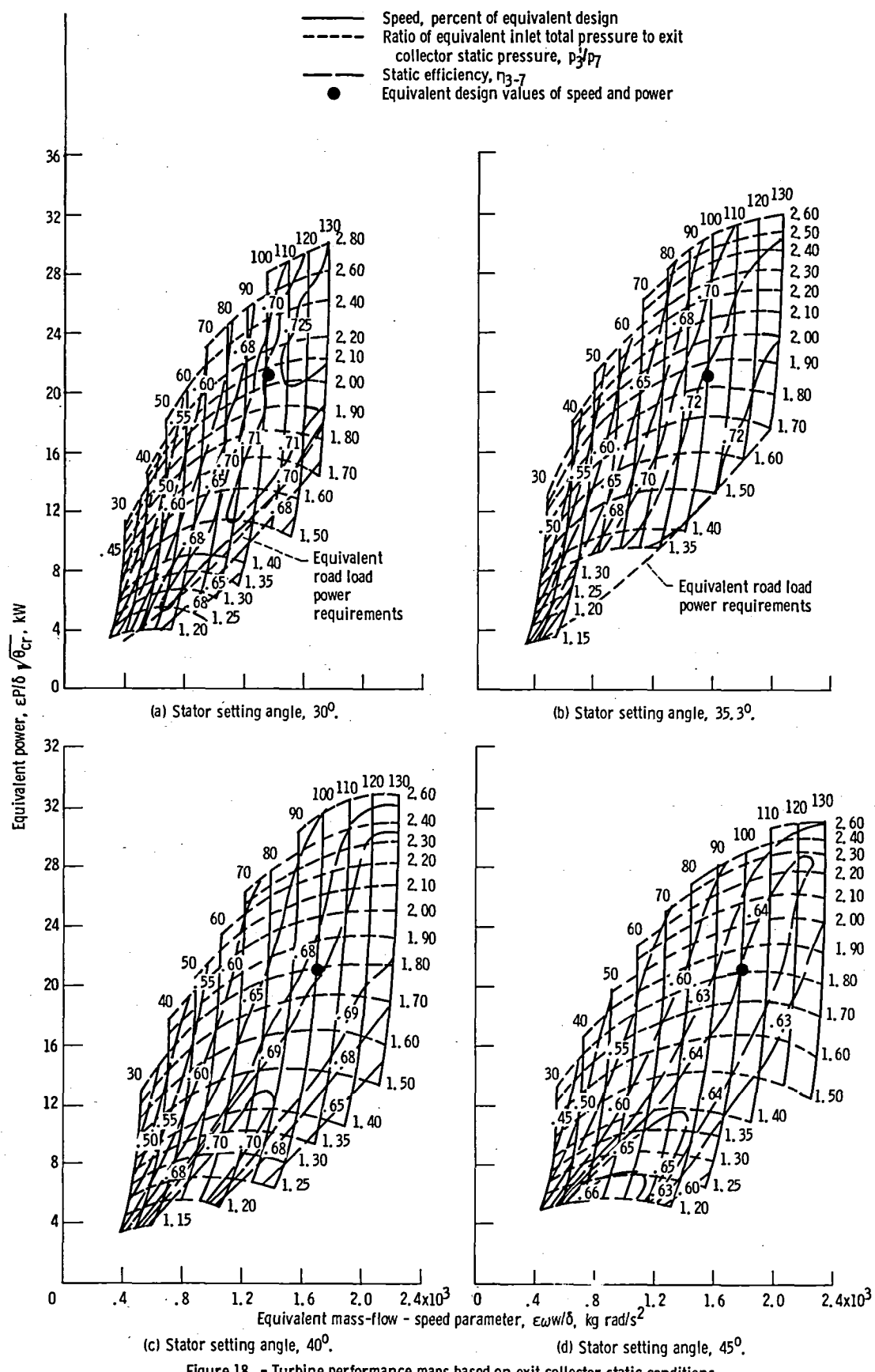


Figure 18. - Turbine performance maps based on exit collector static conditions.

efficiency η_{3-5} of about 0.72 was measured at setting angles of 30° and 35.3° (figs. 18(a) and (b), respectively). This peak efficiency occurred at the design equivalent values of speed and power for the design setting angle of 35.3° (fig. 18(b)). The design overall stage efficiency was 0.815, about 0.095 greater than the measured value. The overall stage efficiencies at design equivalent values of speed and power for setting angles of 40° and 45° were about 0.68 and 0.64, respectively (figs. 18(c) and (d)).

The high-gear, steady-state, road-load power curve (calculated from design values given in ref. 1) is shown in figures 18(a) and (b) to determine if the engine was operating near the power turbine peak efficiency in actual engine operation, where the stator setting angle can vary between 30° and 35.3° . At a setting angle of 30° (fig. 18(a)) the power turbine was operating near the peak efficiency values for speeds less than 70 percent of design. At 90 percent of design speed (road speed of 90 km/hr) the turbine overall stage efficiency was about 0.69, or 0.02 less than the peak efficiency at this speed. At the design setting angle of 35.3° (fig. 18(b)) the road-load power requirements resulted in turbine operation near peak efficiency values at the given speeds over most of the operating range, even though the power turbine operated at relatively low pressure ratios. At 90 percent of design speed the power turbine overall efficiency was about 0.71, or less than 0.01 below the peak efficiency measured for this speed. Although the overall level of turbine efficiency was 0.09 to 0.10 less than design, the objective of operating the power turbine near peak efficiency conditions was achieved.

The turbine total η_{3-5} , static η_{3-5} , and overall stage η_{3-7} efficiencies are shown in figure 19 as functions of stator setting angle at the design equivalent values of speed and total pressure ratio. This figure shows the trends in efficiency level with stator setting angle (flow area) as well as the effect of the exit diffuser on overall efficiency level. As shown in figure 19 the maximum measured total efficiency occurred at the design stator setting angle of 35.3° . The static and overall stage efficiencies at the setting angle of 30° were within 0.01 of their respective maximum values on this curve. The efficiency decreases as the stator setting angle was increased above design and was probably due to increasing stator inlet flow distortion as described previously.

Diffuser performance. — A high-performance diffuser is essential for acceptable engine cycle efficiency. The subject exit diffuser was designed for "optimum" area ratio (see section **Ducting Description**) for annular diffusers, but the geometry constraints of engine packaging require the flow to be turned from axial to radial for dump into the regenerator. This may have some effect on diffuser performance.

The effects of diffuser kinetic energy recovery on overall power turbine performance can be seen in figure

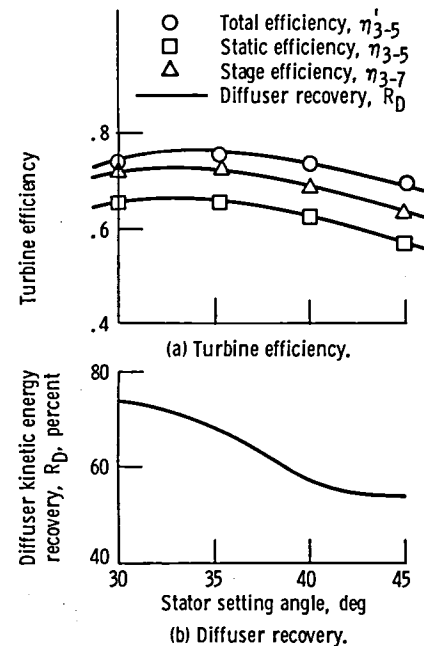


Figure 19. — Variation in turbine efficiency and diffuser recovery for design equivalent values of speed and total pressure ratio.

19. The diffuser recovery was greatest at a stator setting angle of 30° , where 73.7 percent of the rotor exit kinetic energy was recovered. Diffuser recovery decreased with increasing setting angle, and rotor exit absolute velocity level increased with increasing setting angle (increasing stator throat area). The diffuser recovery of 67.3 percent at the design setting angle was near the design value of 67.9 percent.

The static pressure variations through the diffuser on the hub and shroud walls near the design equivalent operating point are shown in figure 20. These conditions correspond to the rotor exit survey point at design setting angle, which is discussed later in the section **Rotor-exit**

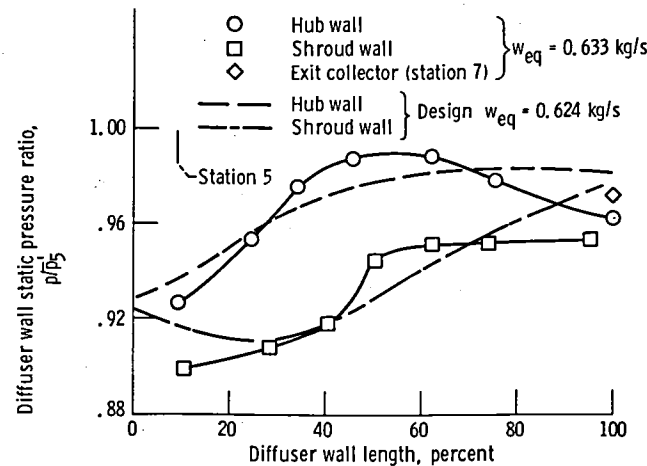


Figure 20. — Variation of wall static pressures through diffuser at equivalent design speed and at a total pressure ratio p_3/p_5 of 1.741.

radial surveys. The total pressure ratio across the blading P'_3/P'_5 of 1.741 was somewhat higher than design. Static pressure increased rapidly on both the hub and the shroud for the first 50 percent of the diffuser wall length. However, the shroud wall static pressure leveled off to a gradual rise to the diffuser exit. The hub wall static pressure rose sharply until 50 to 60 percent of wall length and then decreased to the diffuser exit. This decrease indicates an acceleration of the flow along the hub wall. These trends in wall static pressure are an indication of possible shroud wall flow separation, where the large flow blockage along the shroud wall reduces the effective flow area and thus causes the hub wall static pressure to decrease near the duct exit. The static pressure recovery at this flow condition was 0.535, the design value was 0.580. The pressure recovery to the exit collector was 0.705; the ideal pressure recovery for the design area ratio of 1.9 was 0.723. The effects of diffuser inlet flow distortion and thick boundary layers caused by the turbine blading and the stator inlet flow distortion may account for the pressure recovery being less than the design value, since this value was based on idealized inlet conditions (ref. 9).

The equivalent design wall static pressure variations through the diffuser (ref. 4) are also shown in figure 20. These variations were calculated with the inviscid analysis of reference 6 by using hot dimensions and flow conditions. Except for a region of flow acceleration between 0 and 30 percent of the wall length on the shroud, the wall static pressures increased smoothly from inlet to exit. The trends in wall static pressure that indicate shroud wall flow separation, discussed previously, were not predicted by this inviscid analysis. The design static pressure ratios were higher than the measured ratios at the diffuser inlet and exit because aerodynamic blockage was assumed to be zero in the analytical calculation and because the experimental mass flow rate was 1.5 percent greater than design.

Static pressure through turbine.—The static pressure variations through the turbine stage on the hub and shroud walls are presented in figures 21 and 22, respectively. The local wall static pressure was ratioed to the stator inlet mass-averaged total pressure at each station from the stator inlet (station 3) to the exit collector (station 7). Data are presented at each stator setting angle for equivalent design speed and at setting angles of 30° and 35.3° for 50 percent of equivalent design speed over a range of turbine static pressure ratios P'_5/P'_3 from 0.45 to 0.80.

The hub wall static pressures are shown in figure 21. The static pressure decreased through both the stator (station 3 to station 4) and the rotor (station 4 to station 5) at the hub for all setting angles and pressure ratios tested at equivalent design speed (figs. 21(a) to (d)). At 50 percent of design speed, however, the hub wall static

pressure increased through the rotor for pressure ratios less than design at a setting angle of 30° (fig. 21(e)) but still decreased through the rotor for all pressure ratios at a setting angle of 35.3° (fig. 21(f)). A static pressure decrease through each blade row is desirable to reduce boundary layer growth due to flow deceleration. As stator setting angle increased (stator throat area increased) at any given stage pressure ratio P'_5/P'_3 , the blade row static pressure drop became less in the stator and greater in the rotor.

The rotor static pressure drop can be quantified in terms of a blade row reaction, defined as the change in static pressure across the rotor $P'_4 - P'_5$ as a percentage of the change in static pressure across the stage $P'_3 - P'_5$, where the pressures are either hub wall or tip wall values. At design values of speed and a stage pressure ratio P'_5/P'_3 of 0.536, the rotor hub reactions were 7.4, 20.4, 40.3, and 61.3 percent for setting angles of 30°, 35.3°, 40°, and 45°, respectively. As the stator throat area was increased, more of the stage static pressure drop occurred in the rotor, which means that the flow acceleration became less in the stator and greater in the rotor. At 50 percent of design speed and at design stage pressure ratio, the rotor hub reactions were 0.2 and 12.3 percent for setting angles of 30° and 35.3°, respectively. The hub reactions were lower at 50 percent speed, and the hub reaction at a setting angle of 30° was nearly zero (impulse). At a pressure ratio P'_5/P'_3 of 0.8, which is near the road-load curve for the 30° setting angle at 50 percent of design speed, the rotor hub reaction was -2.3 percent. It should be noted that when total pressure losses are taken into account the rotor hub can have zero reaction when based on static pressure but have a negative value of reaction when based on velocity change. So at a stator setting angle of 30° there was probably flow deceleration at the rotor hub for low speeds and pressure ratios. At the design setting angle and 50 percent of design speed, the rotor hub static pressure reaction remained positive and was 8.3 percent at a stage pressure ratio of 0.8.

The tip wall static pressure variations are shown in figure 22. The wall static pressure decreased through both the stator and the rotor for all pressure ratios and setting angles tested both at design speed and 50 percent of design speed. The trends in blade row static pressure drop were similar to those at the hub in that the stator pressure drop became less and the rotor pressure drop became greater as the stator throat area increased. The static pressure drop at the tip as compared with that at the hub was less in the stator and greater in the rotor. The rotor tip reactions at design values of speed and pressure ratio (P'_5/P'_3 of 0.536) were 32.5, 46.9, 60.2, and 73.7 percent for setting angles of 30°, 35.3°, 40°, 45°, respectively. At design pressure ratio and 50 percent of design speed, the tip reactions were 28.9 and 41.5 percent for setting angles of 30° and 35.3°, respectively. Rotor tip reaction

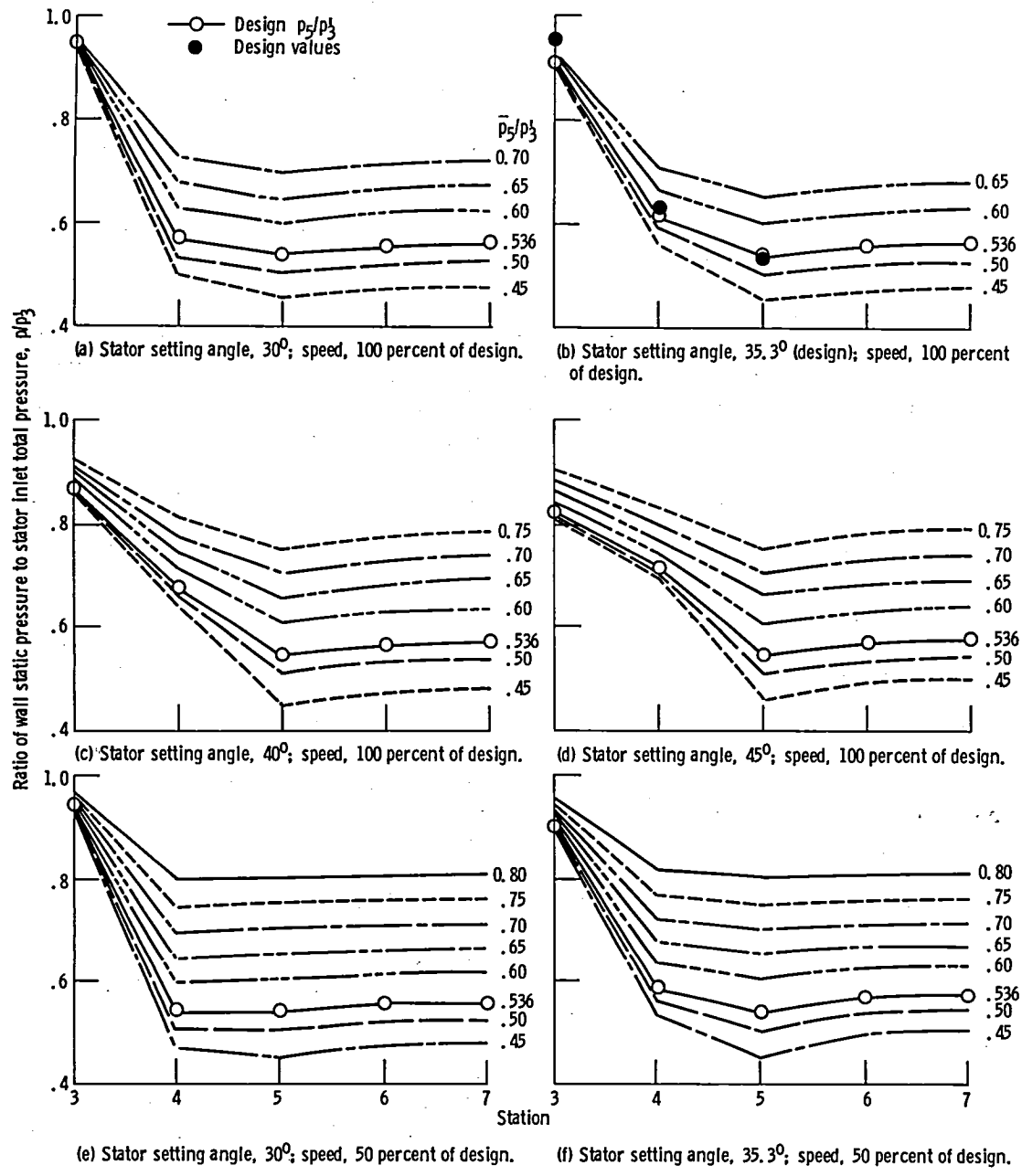


Figure 21. - Variation of hub wall static pressure through turbine.

increased with increasing stator throat area and decreased with decreasing speed.

The level of reaction was high at the tip and should provide adequate flow acceleration through the blade row at all operating conditions to yield low profile losses. However, at high rotor reaction levels tip clearance losses increased significantly because of the increased leakage in the clearance gap, especially for larger tip clearances. This is supported by the limited published data on the effects of reaction on the tip clearance penalty. By using the correlations presented in reference 11, tip clearance penalties due to reaction effects can be approximated.

The penalties in turbine performance due to the high rotor reaction at the 40° and 45° setting angles were calculated to be 0.007 and 0.020, respectively. Of course, the actual performance level achieved as reaction levels increase is a trade-off between decreasing profile losses and increasing tip clearance losses.

The design hub and tip wall static pressures are shown in figures 21(b) and 22(b), respectively, for comparison to measured values. These values are shown at the design ratio of rotor exit static pressure to stator inlet total pressure P_5/P_3 of 0.536. The measured static pressure ratios at the stator inlet and exit were less than the design

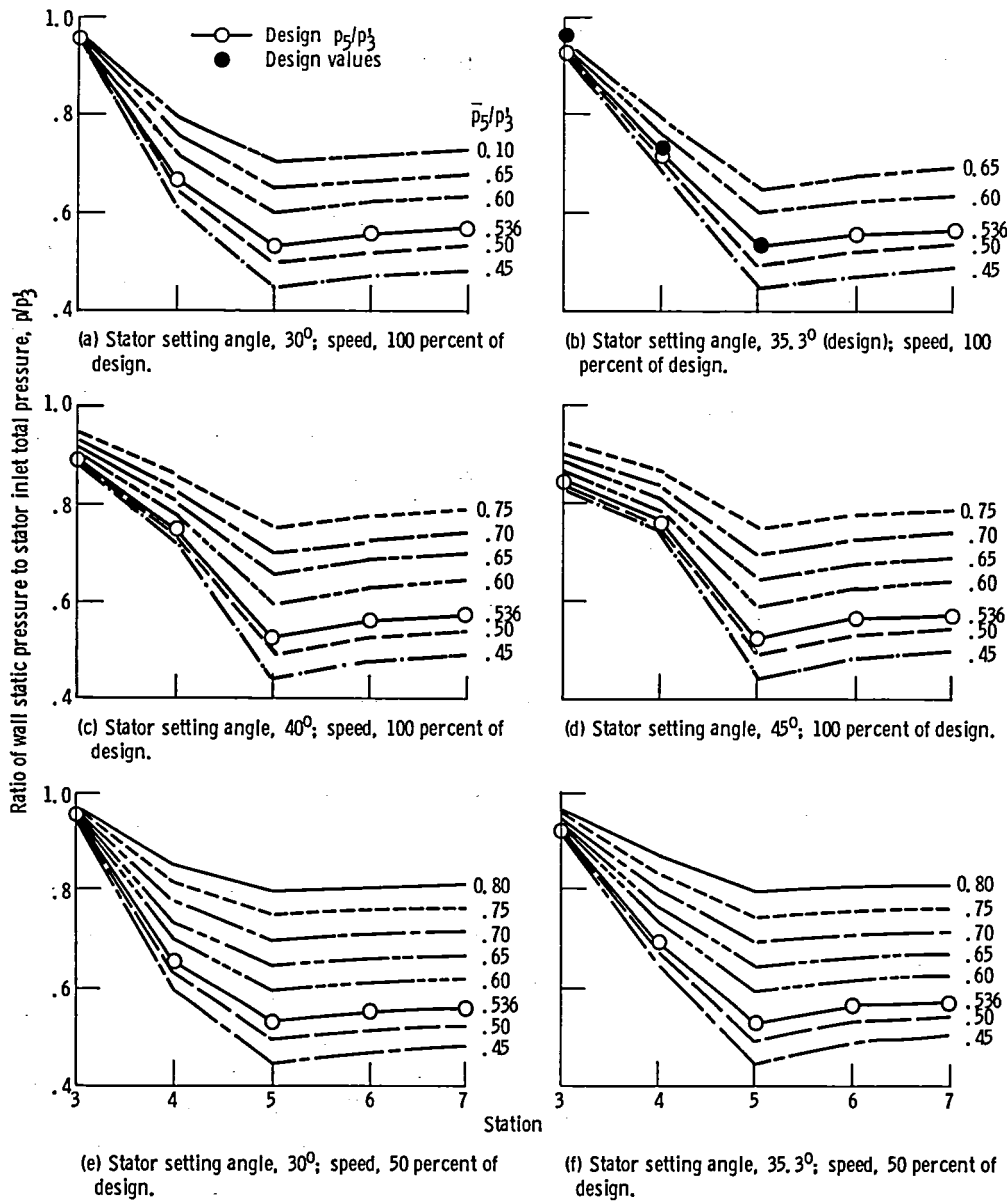


Figure 22. - Variation of outer wall static pressure through turbine.

values on both the hub and tip walls. The lower than design static pressure at the stator inlet was the result of the higher than design mass flow rate and the flow blockage due to the inlet flow distortion. At the stator exit the overexpansion of the flow due to the mismatch in stator and rotor areas, discussed previously, resulted in the lower than design static pressures seen in the figures.

Rotor exit radial surveys.—The rotor exit flow conditions were measured with three radial survey probes, one each at selected circumferential positions as described in the section **Instrumentation**. Probe measurements of flow angle, total temperature, and total pressure were taken at 11 radial positions from hub to tip at equivalent design speed and at total pressure ratios

P_3'/P_5' of 1.73, 1.74, 1.79, and 1.86 for stator setting angles of 30° , 35.3° , 40° , and 45° , respectively. These total pressure ratios differed from each other and from the intended value of 1.712 (design) because the selection of the survey points was based on a total pressure ratio that used a calculated value of inlet total pressure. This calculated value was subsequently found to be 1 to 5 percent lower than the mass-averaged values of inlet total pressure, with the larger differences at the higher mass flow rates. Since the mass-averaged values of inlet total pressure are considered to be more accurate, they were used for all stage data; so the actual survey total pressure ratios were not those intended. This difference should have minimal effect on the intended use of the surveys,

which is to indicate relative performance along the span. The data are presented in terms of absolute flow angle α_5 , total temperature difference $1 - (T_5'/T_3')$, and total efficiency η_{3-5} in figure 23. Stator inlet local conditions were determined at the same stream function values as those calculated for the rotor exit local conditions so as to

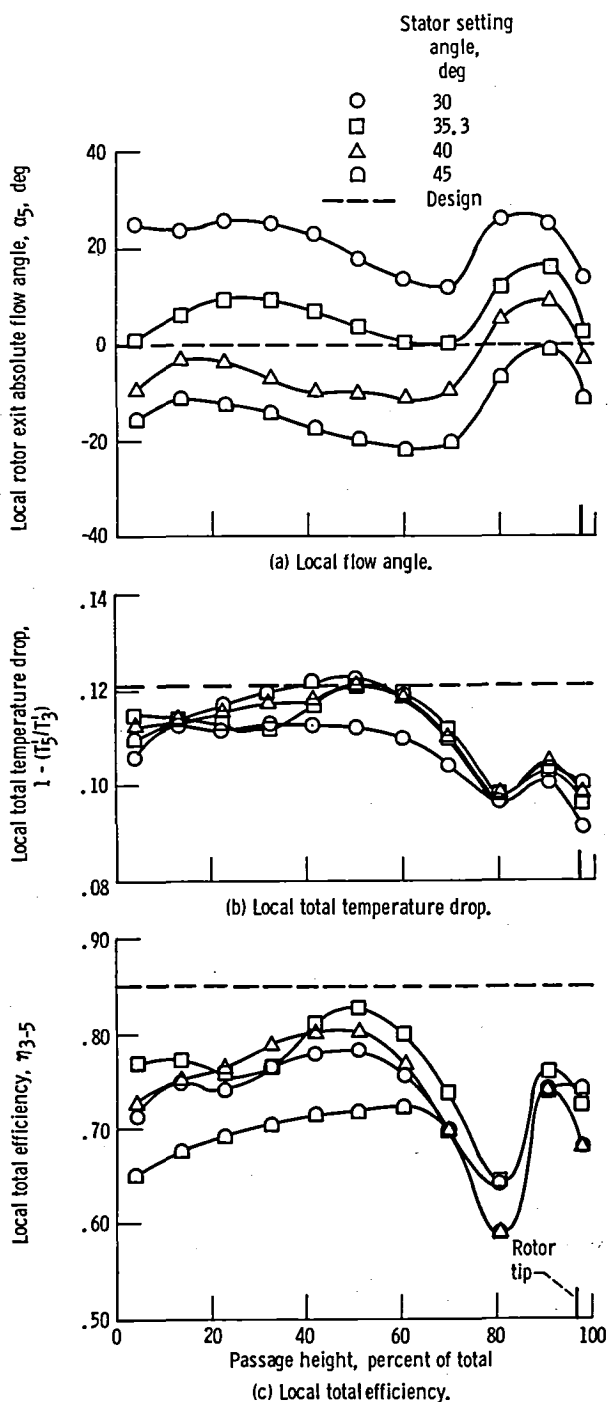


Figure 23. - Variations in rotor exit local flow conditions from survey data taken at equivalent design speed.

present the survey data along quasi-streamlines between the stator inlet and the rotor exit.

The local rotor exit absolute flow angle variations are shown in figure 23(a). As setting angle (stator throat area) increased, the flow angle decreased due to the increasing rotor exit relative velocity. At 50 percent of passage height the flow angles were 18.5° , 4.3° , -10.0° , and -19.3° at setting angles of 30° , 35.3° , 40° , and 45° , respectively. A negative flow angle indicates that the tangential component of absolute velocity is in the direction opposite to rotation and contributes positively to turbine work output. The turbine was designed for zero rotor exit flow angle, but the measured flow angles at the design setting angle were positive over the entire blade passage height. The underturning of the flow was greatest at about 30 and 90 percent of passage height, where the flow angles were about 10° and 16° , respectively. This flow underturning was consistent with the lower than design turbine efficiency (see the section **Turbine Efficiency**) measured at a total pressure ratio of 1.74, which is near the design value of 1.712. The flow angle increased in the tip region from about 70 to 90 percent of passage height for all four setting angles. The large rotor tip clearance (3 percent) caused an unloading of the rotor blades in the tip region, and this trend, shown in figure 23(a), is typical of unshrouded rotors (ref. 11).

The local temperature drop between the stator inlet and the rotor exit is presented in figure 23(b). The temperature variations shown are an indication of the work distribution from hub to tip. Although the work distribution was relatively constant from 10 to 60 percent of the passage height at a setting angle of 30° , the work distributions for the other setting angles had peak values at about 50 percent of the passage height. The radial work distributions for all four stator setting angles differed significantly from the design distribution (dashed line in fig. 23(b)) of constant work from hub to tip especially between 60 and 80 percent of the passage height, where the actual work output decreased sharply.

The variations in local blading total efficiency from hub to tip are shown in figure 23(c) at setting angles of 30° , 35.3° , 40° , and 45° . Maximum efficiency occurred at 50 percent of the passage height for setting angles of 30° , 35.3° , and 40° and at 60 percent for 45° . The maximum values of efficiency for these setting angles were 0.781, 0.827, 0.800, and 0.723, respectively. The design efficiency level of 0.850 was not reached even at midspan at any setting angle. A region of low efficiency existed, centered at about 80 percent of passage height, for all setting angles. Because of the thick boundary layers along the walls at the stator inlet and the low-momentum fluid in those regions, the low-aspect-ratio stator may have generated a vortex core that exited the turbine in this high-loss region. The high efficiency level

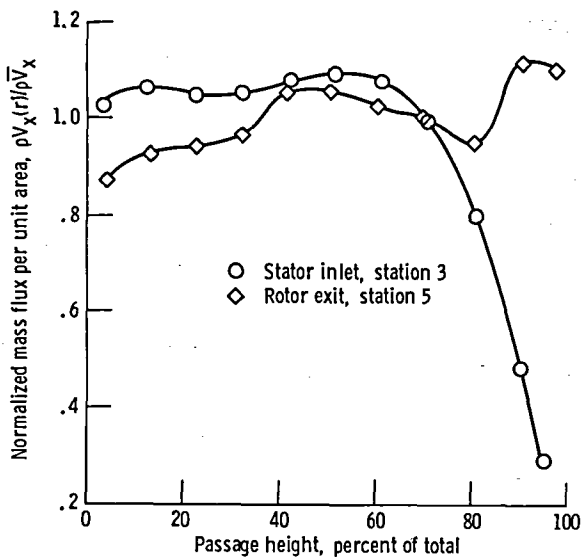


Figure 24. - Comparison of radial variation in mass flux per unit area for stator inlet and rotor exit.

in the tip region was probably due to the flow being redistributed from hub to tip through the turbine so that the rotor exit total pressure was greater than expected in the tip region, considering the large flow distortion near the shroud wall at the stator inlet (fig. 12). This flow redistribution can be seen better in figure 24, which compares the radial variations in mass flux per unit area at the stator inlet and the rotor exit. Although the mass flux was reduced in the hub region as the flow passed from inlet to exit, it was increased in the tip region.

Concluding Remarks

The performance of the power turbine from the DOE 75-kW upgraded automotive gas turbine engine has been presented in this report. This axial-flow power turbine incorporates a variable-area stator that has pivotable vanes for engine control and braking. Other pieces of hardware included in the performance evaluation were the interstage transition duct between the compressor drive and power turbines and the exit diffuser between the power turbine and the regenerator, so that the performance of the turbine stage, as configured in the engine, could be determined.

The aerodynamic goals established during the power turbine design effort were constrained by various mechanical and geometrical requirements perceived as necessary for an automotive gas turbine engine. These constraints on the power turbine design included end clearances for the variable stator vanes, a limited number of stator vanes for mechanical simplicity, large rotor tip clearance to ensure mechanical integrity during thermal transients, and long duct gas paths for smooth transitions

between turbine components. A total efficiency of 0.85 for the power turbine blading was selected on the basis of the available analytical computer codes and the correlated turbine performance data applicable to the selected configuration.

The performance results presented in this report indicate that the turbine blading total efficiency was 0.096 less than the design goal at design equivalent values of speed and total pressure ratio. Stage performance measurements have shown that mass flow rate and turbine torque were 4.35 percent greater than design and 7.0 percent less than design, respectively, for cold hardware dimensions. The stator performance measurements have shown that mass flow rate and stator exit moment of momentum were 3.74 percent higher than design and 3.1 percent less than design, respectively, at the design stator pressure ratio. Since stator and rotor throat areas were measured to be 1.2 percent and 4.3 percent less than design, respectively, the high mass flow rate was due to clearance leakage effects in both the stator and the rotor. Measurement of the interstage duct exit flow conditions has shown large radial gradients in absolute flow angle and total pressure that must have an adverse effect on both stator and rotor aerodynamic performance. Both stator inlet flow distortion and vane-end clearance leakage must be considered significant factors in the poor turbine performance.

Specific problem areas for aerodynamic performance identified in this evaluation and during the design study included stator inlet flow distortion, stator vane-end clearances, low stator aspect ratio, and large rotor tip clearance. However, there are neither adequate analytical tools nor reliable test data available to make the necessary engineering judgments for a small turbine design in which these effects are present.

As the axial-flow turbine is applied to the smaller engine size used in automobiles, trucks, and small helicopters, a major goal will be improving component performance for lower engine specific fuel consumption. To meet this goal, test and analytical research programs to obtain an understanding of the effects of the above-mentioned problem areas on turbine performance will be necessary. The performance evaluation of this automobile power turbine has at least provided a baseline with which component tests, focused on the various problem area, can be compared. Specifically, tests to isolate the effects of inlet flow distortion, vane-end clearances, aspect ratio, and tip clearances should be done on this power turbine configuration.

Summary of Results

Experimentally determined performance data have been presented for the interstage transition duct and the

power turbine stator as well as for the turbine stage and exit diffuser. The results of duct wall static pressure measurements and duct exit radial surveys have been discussed. Stator performance was determined from reaction torque measurements with a stationary paddlewheel rotor at the stator exit, and the results have been presented in terms of mass flow rate and stator exit moment of momentum for vane-chord setting angles of 30°, 35.3°, 40°, and 45°. The power turbine stage performance was determined at stator setting angles of 30°, 35.3°, 40°, and 45° in terms of mass flow rate, torque, speed, power, and efficiency. The variations in hub and shroud wall static pressures through the turbine have been presented as well as the radial variation in rotor exit flow conditions at each stator setting angle. The exit diffuser performance has been presented at design conditions in terms of the wall static pressure variations through the diffuser. The results of this investigation are summarized as follows:

1. The interstage duct produced large radial gradients in flow conditions at the stator inlet that increased with increasing mass flow rate. The measured pressure recovery of 0.559 was less than the design value of 0.570.

2. The measured equivalent values of mass flow rate and exit moment of momentum for the stator at design values of setting angle and pressure ratio (P_4/P_3 of 0.685) were 0.624 kg/s and 13.81 m²/s, respectively. These values are respectively, 3.7 percent higher and 3.1 percent lower than the design values for cold dimensions.

3. The measured equivalent turbine mass flow rate was 0.6277 kg/s at equivalent design values of speed and static pressure ratio (P_3/P_5 of 1.867) for a stator setting angle of 35.3° (design). This value is 4.35 percent greater than the design value for cold dimensions.

4. The measured equivalent torque was 7.97 N-m at equivalent design values of speed and static pressure ratio for a stator setting angle of 35.3°. This value is 7.0 percent less than the design value for cold dimensions.

5. The combination of a torque 7.0 percent less than design with a mass flow rate 4.35 percent greater than design resulted in an equivalent specific work 11.35 percent less than design and a static efficiency 0.084 less than the design value of 0.741.

6. For design equivalent values of speed and total pressure ratio (P_3/P_5 of 1.712) at the design setting angle of 35.3°, the turbine total η_{3-5} , static η_{3-5} , and stage η_{3-7}

efficiencies were 0.754, 0.657, and 0.723, respectively. The total efficiency was 0.096 less than design.

7. A peak total efficiency of 0.76 was measured at both 30° and 35.3° stator setting angles.

8. The power turbine steady-state operating line corresponding to the road-load power curve was within 0.02 of the peak stage efficiency at a given turbine speed.

9. The static pressure recovery of the exit diffuser was 0.535 at near equivalent design conditions, while the design value was 0.580. The nonuniform flow conditions at the rotor exit were probably responsible for the low measured pressure recovery.

References

1. Ball, G. A.; Gumaer, J. I.; and Sebestyen, T. M.: The ERDA/Chrysler Upgraded Gas Turbine Engine—Objectives and Design. SAE 760279, 1976.
2. Galvas, Michael R.: Compressor Design for the Energy Research and Development Agency (ERDA) Automotive Gas Turbine Program. NASA TM X-71719, 1975.
3. Roelke, Richard J.; and McLallin, Kerry L.: The Aerodynamic Design of a Compressor-Drive Turbine for Use in a 75 kW Automotive Engine. NASA TM X-71717, 1975.
4. Kofskay, Milton G.; Katsanis, Theodore; and Schumann, Lawrence F.: Aerodynamic Design of a Free Power Turbine for a 75 kW Gas Turbine Automotive Engine. NASA TM X-71714, 1975.
5. Miser, James W.; Stewart, Warner L.; and Whitney, Warren J.: Analysis of Turbomachine Viscous Losses Affected by Changes in Blade Geometry. NACA RM E56F21, 1956.
6. Katsanis, Theodore; and McNally, William D.: FORTRAN Program for Calculating Velocities and Streamlines on the Hub-Shroud Mid-Channel Flow Surface of an Axial- or Mixed-Flow Turbomachine. I: Users Manual. NASA TN D-7343, 1973.
7. Katsanis, Theodore: FORTRAN Program for Calculating Transonic Velocities on a Blade-to-Blade Stream Surface of a Turbomachine. NASA TN D-5427, 1969.
8. Kofskay, Milton G.: Experimental Investigation of Three Tip Clearance Configurations Over a Range of Tip Clearance Using a Single-Stage Turbine of High Hub-to-Tip Radius Ratio. NASA TM X-472, 1961.
9. Sovran, Gino; and Klomp, Edward D.: Experimentally Determined Optimum Geometries for Rectilinear Diffusers with Rectangular, Conical, or Annular Cross-Section. Fluid Mechanics of Internal Flow, G. Sovran, ed., Elsevier Publishing Co. (Amsterdam), 1967, pp. 270-319.
10. Kofskay, Milton G.; and McLallin, Kerry L.: Cold-Air Performance of Free Power Turbine Designed for 112-Kilowatt Gas-Turbine Engine. III. Effect of Stator Vane End Clearances on Performance. NASA TM-78956, DOE/NASA/1011-78/29, 1978.
11. Glassman, Arthur J., ed: Turbine Design and Application. NASA SP-290, Vol. II, 1973.

1. Report No. NASA TM-82644	2. Government Accession No.	3. Recipient's Catalog No.	
4. Title and Subtitle COLD-AIR PERFORMANCE OF A 15.41-cm-TIP-DIAMETER AXIAL-FLOW POWER TURBINE WITH VARIABLE-AREA STATOR DESIGNED FOR A 75-kW AUTOMOTIVE GAS TURBINE ENGINE		5. Report Date February 1982	
7. Author(s) Kerry L. McLallin, Milton G. Kofskey, and Robert Y. Wong		6. Performing Organization Code 778-32-01	
9. Performing Organization Name and Address National Aeronautics and Space Administration Lewis Research Center Cleveland, Ohio 44135		8. Performing Organization Report No. E-899	
12. Sponsoring Agency Name and Address U. S. Department of Energy Vehicle and Engine R&D Washington, D. C. 20585		10. Work Unit No.	
		11. Contract or Grant No.	
		13. Type of Report and Period Covered Technical Memorandum	
		14. Sponsoring Agency Code Report No. DOE/NASA/51040-30	
15. Supplementary Notes Final report. Prepared under Interagency Agreement DE-AI01-77CS51040.			
16. Abstract <p>An experimental evaluation of the aerodynamic performance of the axial-flow, variable-area-stator power turbine stage for the Department of Energy upgraded automotive gas turbine engine was conducted in cold air. The interstage transition duct, the variable-area stator, the rotor, and the exit diffuser were included in the evaluation of the turbine stage. The measured total blading efficiency was 0.096 less than the design value of 0.85. Large radial gradients in flow conditions were found at the exit of the interstage duct that adversely affected power turbine performance. Although power turbine efficiency was less than design, the turbine operating line corresponding to the steady-state road-load power curve was within 0.02 of the maximum available stage efficiency at any given speed.</p>			
17. Key Words (Suggested by Author(s)) Variable-area stator Axial-flow turbine Gas turbine engine Experimental performance		18. Distribution Statement Unclassified - unlimited STAR Category 07 DOE Category UC-96	
19. Security Classif. (of this report) Unclassified	20. Security Classif. (of this page) Unclassified	21. No. of Pages 33	22. Price* A03

* For sale by the National Technical Information Service, Springfield, Virginia 22161



National Aeronautics and
Space Administration

Washington, D.C. SPECIAL FOURTH CLASS MAIL
20546 BOOK

Postage and Fees Paid
National Aeronautics and
Space Administration
NASA-451

Official Business
Penalty for Private Use \$300



Postage and Fees Paid
National Aeronautics and
Space Administration
NASA-451



1 13 1U,A, 032982 S00008ASR

LANGLEY RESEARCH CENTER
ATTN: TECHNICAL LIBRARY, MS 185
HAMPTON VA 23665



POSTMASTER: If Undeliverable (Section 158
Postal Manual) Do Not Return
